Defence Research and Development Canada
Recherche et développement pour la défense Canada

DEFENCE R&D DÉFENSE

Measurement of toxic industrial chemicals, chemical warfare agents and their simulants

A LWIR passive standoff detection study

H. Lavoie
E. Puckrin
J.-M. Thériault
D. Dubé
DRDC Valcartier

Defence R&D Canada – Valcartier
Technical Report
DRDC Valcartier TR 2006-634
April 2007

Canada

Measurement of toxic industrial chemicals, chemical warfare agents and their simulants

A LWIR passive standoff detection study

H. Lavoie
E. Puckrin
J.-M. Thériault
D. Dubé
DRDC Valcartier

Defence R&D Canada – Valcartier

Technical Report
DRDC Valcartier TR 2006-634
April 2007

Principal Author

Hugo Lavoie Ph.D. D.Sc.

Defence scientist

Approved by

Jean-Marc Garneau Ph.D.

C/S Optronic Surveillance

Approved for release by

Christian Carrier

Chief Scientist

[Include the sponsor of the work or a reference to a thrust or work unit, when deemed appropriate by author or CSA; relevant patent number(s), relating to protected intellectual property, should be noted. If there is no relevant information for this document, delete this text.]

Abstract

This report presents a summary of the measurements performed using the Compact ATmospheric Sounding Interferometer (CATSI) for the standoff detection of toxic chemical vapours at DSTL, Porton Down, UK in June 2005. This work is based on the passive standoff detection of chemical warfare agent (CWA) simulants such as SF_6, NH_3 and TEP; precursors such as DMMP; and toxic chemical vapours such as phosgene and GB. The measurements were performed for a variety of concentrations and at low thermal contrast in an open-air environment. Some chemicals were released in the presence of yellow smoke to act as an obscurant. The measurements collected during the trial were used to evaluate the performance and capability of the CATSI sensor for detecting, identifying and quantifying a chemical vapour cloud at distances between 500 m and 1.5 km. The results show that CATSI was able to detect and identify all of the chemical vapours released during the trial, including the CWA. The measurements made in the presence of yellow smoke provide some preliminary evidence that some obscurants do not significantly affect the detection capability of a passive standoff sensor. The measurements of GB in the field also demonstrate that the atmosphere has an insignificant effect on the signature of the pure agent. The work performed in this field trial is also useful for validating the approach and methodology used in the new engineering development model of the CATSI system (CATSI-EDM), which will be made available to the CF in 2007.

Résumé

Ce rapport présente un résumé des mesures qui ont été effectuées à l'aide du radiomètre spectral CATSI (Compact ATmospheric Sounding Interferometer) lors de l'essai de détection en retrait de vapeurs toxiques et de simulants qui a eu lieu en juin 2005 à DSTL, Porton Down en Angleterre. Ce travail est basé sur la détection en retrait de simulants d'agents chimiques tels que SF_6, NH_3 et TEP, de précurseurs tels que le DMMP et sur des vapeurs toxiques de phosgène et GB. Les mesures ont été effectuées à différentes concentrations et à faibles contrastes thermiques dans un environnement à ciel ouvert. Les mesures obtenues au cours de l'essai ont permis d'évaluer les performances et les capacités de CATSI à détecter, identifier et quantifier un nuage de vapeur chimique à une distance entre 500 m et 1,5 km. Les résultats montrent que CATSI a été capable de détecter et d'identifier toutes les vapeurs chimiques et les agents chimiques libérés dans l'atmosphère. Les mesures effectuées en présence de fumée jaune ont fourni des évidences que certains obscurcissants n'affectent pas de façon significative les capacités de détection des capteurs passifs en retrait. Les résultats obtenus avec le GB en milieu ouvert ont aussi démontré que l'atmosphère n'avait aucun effet sur la signature des agents de combat. Cet essai a aussi été très utile pour la validation de l'approche et de la méthodologie utilisées pour le projet de développement d'un modèle militarisé de CATSI (CATSI-EDM) dont les Forces canadiennes pourront disposer en 2007.

This page intentionally left blank.

Executive summary

Measurement of toxic industrial chemicals, chemical warfare agent and their simulants: A LWIR passive standoff detection study

Lavoie, H., E. Puckrin, J.-M. Thériault and D. Dubé; DRDC Valcartier TR 2006-634; Defence R&D Canada – Valcartier; April 2007.

Background

The passive standoff detection, identification and quantification of chemical warfare agents (CWA) at distances up to five kilometres may offer operational benefits. These include early warning of CWA attack, reconnaissance and fixed-site monitoring. The detection of CWAs and toxic industrial chemicals (TICs) at the greatest possible range gives the opportunity to the Canadian Forces (CF) to be prepared for these threats. The detection of chemical threats with passive standoff detection techniques has been an important field of interest for the last decade. This report summarizes the results of a field trial held in June 2005 at DSTL, Porton Down, UK. This work is based on the passive standoff detection of CWA simulants such as SF_6, NH_3 and TEP; precursors such as DMMP; and toxic chemical vapours such as phosgene and GB in an open-air environment.

Results

The report shows that chemical vapour clouds were detected at distances of 500 metres to 1.5 kilometres with the Compact ATmospheric Sounding Interferometer (CATSI) sensor. Some chemicals were released in the presence of yellow smoke to act as an obscurant. The results show that CATSI was able to detect and identify all of the chemical vapours released during the trial, including the CWA. The measurements made in the presence of yellow smoke provide some preliminary evidence that some obscurants do not significantly affect the detection capability of a passive standoff sensor. The measurements of GB in the field also demonstrate that the atmosphere has an insignificant effect on the signature of the pure CWA.

Significance

The work done in this field trial is part of the validation of the passive standoff detector built for the CATSI-EDM project. This report will show the capability of the CATSI approach to detect and identify CWAs, their precursors and TICs on the battlefield.

Future plans

The development of a passive long wave infrared (LWIR) standoff detector for the military environment is now a priority. The CATSI-EDM project is the first effort to provide this kind of technology to the battlefield.

This page intentionally left blank.

Sommaire

Measurement of toxic industrial chemicals, chemical warfare agent and their simulants: A LWIR passive standoff detection study

Lavoie, H., E. Puckrin, J.-M. Thériault and D. Dubé; DRDC Valcartier TR 2006-634; R & D pour la défense Canada – Valcartier; March 2007.

Introduction ou contexte

La détection, l'identification et la quantification d'agents chimiques de combat (CWA) à une distance au delà de 5 km par méthode passive pourrait constituer un avantage opérationnel. Cela comprend la détection rapide d'attaques par CWA, la reconnaissance et la surveillance des lieux. La détection de CWA et de composés industriels toxiques (TIC) à grande distance permettra aux Forces canadiennes d'être prêtes à contrer cette menace. La détection de menaces chimiques par la méthode de détection passive en retrait a été un champ d'étude important au cours de la dernière décennie. Ce rapport présente un résumé des résultats obtenus lors d'essais qui ont eu lieu en juin 2005 à DSTL, Porton Down, en Angleterre. Ce travail est fondé sur la détection en retrait dans un environnement ouvert par méthode passive de simulants tels que le SF_6, NH_3 et le TEP, un précurseur (DMMP) ainsi que de gaz chimiques toxiques tels que le phosgène et le GB.

Résultats

Ce rapport décrit la détection, à l'aide de CATSI (Compact Atmospheric Sounding Interferometer), de nuages de vapeurs chimiques à une distance entre 500 mètres et 1,5 kilomètre. Certains composés ont été libérés en présence de fumée jaune agissant comme un obscurcissant. Les résultats montrent que CATSI a été en mesure de détecter et d'identifier toutes les vapeurs chimiques, incluant les CWA libérés lors de cet essai. Les mesures effectuées en présence de fumée jaune ont fourni la preuve que certains obscurcissants n'affectaient pas de façon significative les capacités des capteurs passifs en retrait. Les résultats obtenus avec le GB à ciel ouvert ont aussi démontré que l'atmosphère n'avait aucun effet sur la signature des CWA.

Importance

Ce travail sur le terrain fait partie de la validation de la technique de détection passive en retrait qui est la base du projet CATSI-EDM. Ce rapport montre les capacités de l'approche CATSI à détecter et identifier les CWA, leurs précurseurs et les TIC sur le champ de bataille.

Perspectives

Le développement de spectromètres passifs dans l'infrarouge thermique (LWIR) pour la détection en retrait dans un environnement militaire est maintenant une priorité. Le projet CATSI-EDM est le premier effort permettant d'amener cette technologie sur le champ de bataille.

This page intentionally left blank.

Table of contents

List of figures

List of tables

Acknowledgements

The authors would like to thank Dr. Anita Jones, the trial organizer at DSTL, Porton Down, for the invitation to participate in this trial. We would also like to express our gratitude to all DSTL (Porton Down) and range personnel for the support they provided during the trial.

This page intentionally left blank.

1. Introduction

The passive standoff detection and identification of chemical warfare agents (CWA) at long distances from the sensor may offer important operational benefits. These include early warning of CWA attack, reconnaissance and fixed-site monitoring. Chemical threats in an operational theatre (e.g., battlefields, towns, peacekeeping missions or industrial gas emission surveillance) are very dangerous to both the general public and the soldiers deployed on the operation. The detection of CWAs and toxic industrial chemicals (TICs) is necessary in order to prepare the Canadian Forces (CF) for this kind of threat. The detection of chemical threats with passive standoff detection techniques has been an important field of research in the last decade.

There are several difficulties associated with passive standoff detection in the long wave infrared (LWIR) region: 1. the suppression of the background signal, which typically represents 95% to 99% of the total signal collected by the detector, 2. the need for a thermal difference between the background and the target gas, and 3. the variable self-emission from the spectrometer. As a result of these limitations, it is difficult to detect a threat at a distance of several kilometres with a passive standoff sensor.

The Compact ATmospheric Sounding Interferometer (CATSI) was developed at DRDC Valcartier to improve the CF surveillance and detection capability against chemical threats. The double-input beam capability of the CATSI spectrometer gives the opportunity to subtract the background clutter from the total input signal in real time [1-7], leaving the target signature.

This report summarizes the results of a field trial held at the Defence Science and Technology Laboratory (DSTL), Porton Down, UK in June 2005. This field trial presented a valuable opportunity to measure the signatures of several CWA simulants (SF_6, ammonia, DMMP and TEP), toxic materials (phosgene) and chemical warfare agent (GB) in an open-air environment. Some measurements were taken in the presence of yellow smoke, which added an operational field obscurant. This report summarizes the performance and capability of the CATSI sensor for detecting, identifying and quantifying a chemical vapour cloud at distances of 500 m to 1.5 km. The work performed in this field trial is also useful for validating the approach and methodology used in the new engineering development model of the CATSI system (CATSI-EDM), which will be made available to the CF in 2007.

2. Material and methods

2.1 Passive standoff detection principle

Figure 1 shows the principle and the critical elements of the passive standoff detection technique. A chemical cloud in the atmosphere can be detected when a thermal contrast between the air (target cloud) and the background is observed within the thermal infrared region (715 to 1400 cm^{-1} or 14 to 7 μm, respectively). This thermal contrast is critical, since the sensibility and quality of the detection are directly related to it.

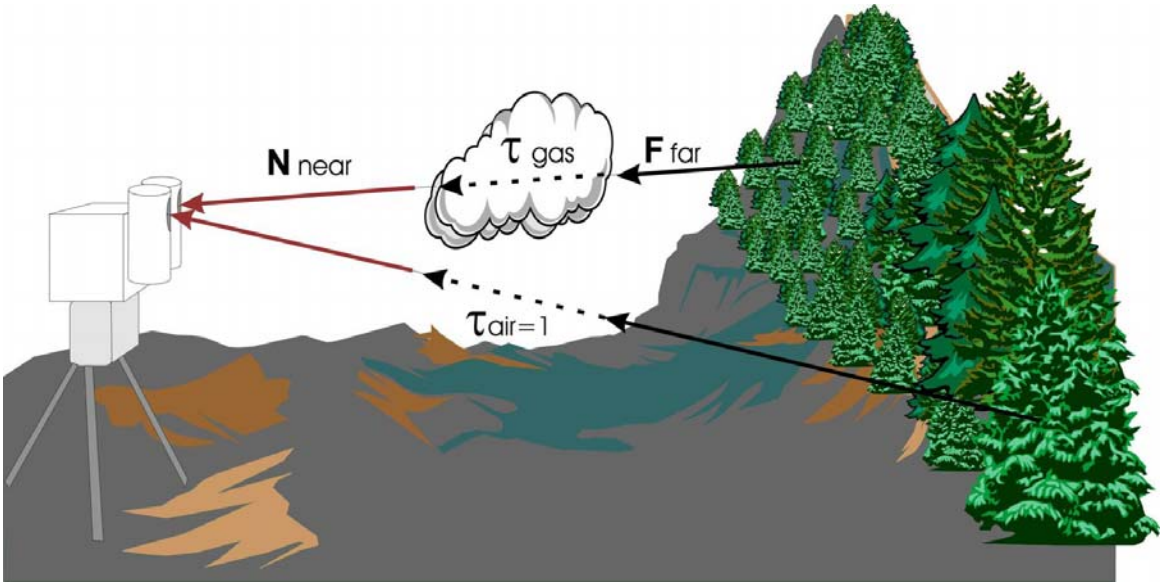

Figure 1: Typical operation of a passive standoff sensor such as CATSI

2.1.1 Detection method

Figure 2 is a diagram of the 3-layer geometry model that describes the differential detection method using a double-beam interferometer like CATSI. Both detection modes (direct and differential) will subtract the background (F_{far}) and atmospheric (N_{near}, τ_{near} and τ_{air}) components from the total input signal; however, the direct mode may introduce temporal fluctuations. Equation (1) is based on the parameters denoted in Figure 2 where L_{gas} , B_{gaz} and τ_{gas} are respectively the total path radiance, the Planck radiance and the transmittance associated with the target gas layer. The transmittance of the air layer (between z_1 and z_2) is given by τ_{air}, and N_{near} and τ_{near} are respectively the near-field path radiance and the transmittance of the atmosphere. The total path radiance without target gas (L_{clear}) and the far-field radiance (F_{far}) are terms which are often quite difficult to evaluate. These difficulties are reduced by the capability of CATSI to subtract optically in real time the background (atmosphere and clutter) from the total path radiance, L_{gas}. The result of the optical subtraction (δL_{calc}) is given by equation (2).

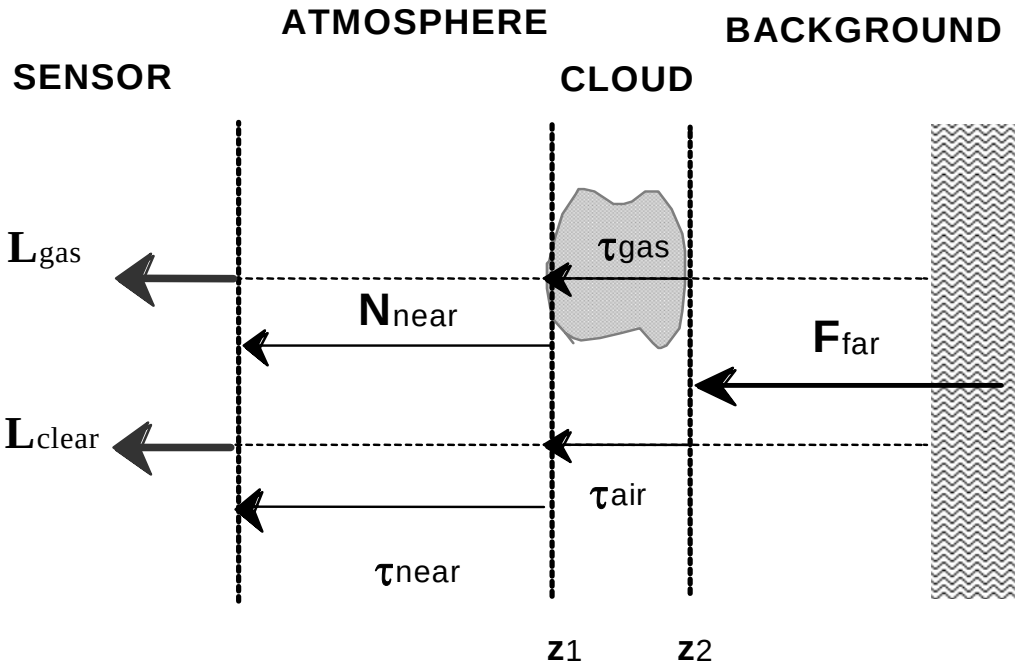

Figure 2: Diagram of the 3-layer geometry for the differential detection of chemical cloud

$$\delta L_{calc} \equiv L_{gas} - L_{clear} = \left(1-\tau_{gas}\right)\left[B_{gas}\tau_{near} + N_{near} - L_{clear}\right] \tag{1}$$

Equation (1) describes an ideal scenario (Figure 2) where the background is constant over the acquisition for the sequential (direct) and the simultaneous (differential) detection. Finally, it can be verified that if a chemical cloud occupies a fraction, f , of the sensor field of view (FOV), the differential radiance can be calculated by:

$$\delta L_{calc} \equiv L_{gas} - L_{clear} = \Delta L_{clear} + f\left(1-\tau_{gas}\right)\left(B_{gas}\tau_{near} + N_{near} - L_{clear} - \Delta L_{clear}\right) \tag{2}$$

τ_{gas} is related to the integrated path concentration (CL) by the Beer-Lambert law:

$$\tau_{gas} = \exp^{(-\alpha_v CL)} \tag{3}$$

Where α_v is the absorption coefficient as a function of frequency (in 1/ppm m), C is the volumic concentration in ppm and L is the path length of the gas target in metres. The measure of interest, *CL*, is expressed in ppm m.

For more details on the detection method and other scenarios, see references [1, 2, 5].

2.1.2 Description of the CATSI sensor

In the passive standoff detection approach the monitoring procedure takes advantage of the differential detection capability provided by an optimized double-beam interferometer (CATSI) with adjacent fields of view [2, 8]. In this system, two beams of thermal radiation originating from different scenes can be optically combined onto a single detector and subtracted in real time. Thus, if one beam entering the interferometer corresponds to the target-plus-background scene and the other corresponds to a consistent background scene, then the resulting differential spectrum corresponds primarily to the target scene minimally perturbed by the background. The standard configuration for the CATSI sensor consists of two identical Newtonian telescopes (Figure 3), each with a diameter of 10 cm, which are optically coupled to the double-beam interferometer (Bomem-type instrument). Each telescope can be individually aimed at a selected scene, i.e., one at the target cloud scene and the other at a cloud-free background scene. This system allows measurements of spectra to be made according to the following specifications: 1. scene field of view (FOV) of 11 mrad or less, 2. spectral coverage from 7 to 14 μm, and 3. a maximum spectral resolution of 1 cm^{-1}. Coarse and fine adjustments in azimuth and elevation are simply achieved by rotating the whole assembly, which is installed on a pan-and-tilt mount positioned on a tripod. Additional information on the CATSI and its radiometric calibration has been reported elsewhere [2, 8].

Figure 3: CATSI sensor with the 10 cm telescopes used for this trial.

This page intentionally left blank.

3. Description of the trial

3.1 Description of the scenes

The passive standoff detection field trial was held at DSTL, Porton Down, UK in June 2005. Figure 4 shows the range used for the trial with the dissemination equipment at the bottom of the bowl. The picture was taken from the point where the passive standoff detectors were located. The chemical release points were situated at 500 m in the bottom of the bowl (photo) and on the high ground closer to the trees at distances up to 1.4 km.

Figure 5 shows the field and the equipment used for the constrained dissemination of the CWA (GB) taken from a similar vantage point. The cloche situated at the centre-left of the photo (white plastic tunnel) was built to produce and stabilize the CWA cloud. At the front end (left side of the cloche), a large fan was positioned to extract the CWA cloud from the cloche and form a plume. A water curtain was located 25–50 m from the front side of the cloche to stop the progression of the CWA plume. The water curtain was activated 20 to 30 s before the release of the agent.

Figure 4: Photo of the field showing the simulant release points

Figure 5: Photo of the field with the semi-constrained dissemination structure (cloche) for the GB release.

3.2 Description of gases released

Table 1 lists the chemical products and dissemination methods used during this trial. For more information, refer to the field trials protocol [9]. Chemical substances in gas phase (SF_6 and NH_3) were released directly from gas tanks. A wide range of flow rates and release amounts were used with all gases as described in Table 1. The chemical products in liquid phase (DMMP and TEP) were disseminated continuously with a spray technique. Table 1 presents the flow rates and the total amounts released for all episodes of this trial.

Two methods were used to release the phosgene. The first method involved the gaseous release of the chemical from a tank, and the second method was similar to a military scenario where the chemical was released with an explosion. The explosive releases were obtained by detonating a phosgene cylinder wrapped with an explosive ribbon, which resulted in the instantaneous dissemination of the gas.

The release of the CWA Sarin (GB) was semi-constrained within the cloche and disseminated with an electric fan to eject the chemical vapour. The agent was placed on a hot plate to vaporize it and form a cloud in the cloche.

***Table 1: C**hemicals released as presented in this report*

Chemical name	Date/time	Flow rate (*kg/min*)	Document section[1]	Standoff distance[2] (*metres*)	Dissemination method
Sulphur hexafluoride (SF_6)	June 09, 14:47	1.4	4.1.1	870	Continuous
	June 17, 15:26	0.15	4.1.1	1440	Continuous
	June 09, 15:01	1.25[3]	4.1.2	870	Continuous[3]
Ammonia (NH_3)	June 09, 15:18	0.825	4.1.3	870	Continuous
	June 09, 15:24	0.8	4.1.4	870	Continuous
Dimethyl methylphosphonate (DMMP)	June 21, 12:29	0.5	4.2.1	645	Continuous
Triethyl phosphate (TEP)	June 21, 15:35	0.6	4.2.2	635	Continuous
Phosgene (CG)	June 13, 12:13	1.2	4.3.1	870	Continuous
	June 17, 14:05	6.0	4.3.2	870	Instantaneous
	June 28, 15:40	3.0	4.3.2	1530	Instantaneous
Sarin (GB)	June 30, 19:05	0.15[4]	4.4	485	Cloche

[1] Reference.

[2] Distance between release point and sensors.

[3] Release masked by yellow smoke.

[4] Total amount.

3.3 Meteorological Conditions

All releases except those involving GB consisted of the unconstrained dissemination of the chemical. For this reason, the meteorological conditions were specified for each release to

minimize the hazard propagation distance. The weather conditions for release were prescribed in section 6 of the field trials protocol for each chemical compound. For more information refer to [9].

4. Results

This section describes the results of the measurements performed during the trial held in June 2005 at DSTL Porton Down. The results are classified according to whether the chemical release involved a gaseous CWA simulant, a liquid CWA simulant, a TIC or a real CWA. Each result acquired by CATSI for a particular release is displayed using two methods: an overlay graphic of all spectra displayed on the same scale in 2D, and a spectrogram showing the radiance intensity as a function of frequency and time derived from a composite of all the measurements for a specific release. These results are supplemented with figures representing the quality of the fit (r^2) and the column density (CL in ppm m) associated with the release, as computed with the GASEM algorithm. For some measurements, a figure containing a Gaussian plume simulation [10, 11] is presented to allow comparison with the column density obtained with the GASEM algorithm developed by DRDC Valcartier [1, 2, 5]. These figures also give an idea of how much of the FOV is filled by the chemical vapour release as a function of the release point distance from the sensor.

4.1 CWA simulant (gas)

4.1.1 Pure sulphur hexafluoride (SF_6)

Figure 6 shows the results obtained for a release of SF_6 at a flow rate of 1.4 kg/min for 1 min at a distance of 870 m from the sensor. The overlay plot and the spectrogram of the differential radiance show the entire series of spectra collected by CATSI during the release period, which occurred at 14:47 local time (LT) on June 9, 2005. The background for this measurement consisted mostly of grass, and the temperature contrast (ΔT) between the background and the air was evaluated at 1.3 K (see [2] for ΔT evaluation method). The overlay plot presented in Figure 6 (left panel) shows several spectra where the SF_6 gas can be clearly detected and identified. The band at 945 cm^{-1} is characteristic of SF_6 and fits with the SF_6 signature shown in Figure 7. The spectrogram presented in Figure 6 (right panel) shows the evolution of the radiance as a function of time. The 940–950 cm^{-1} region of the spectrogram shows clearly the evolution of the SF_6 band in the interval between 40 and 140 s with a good signal-to-noise ratio (SNR). The red streak perpendicular to the time axis (between 75 s and 85 s) is attributed to intensity fluctuations as shown on the overlay plot. This streak can be explained by a change in the background temperature due to clouds moving over the scene or by the scanning procedure where the FOV moves from a hot background to a colder one (sky).

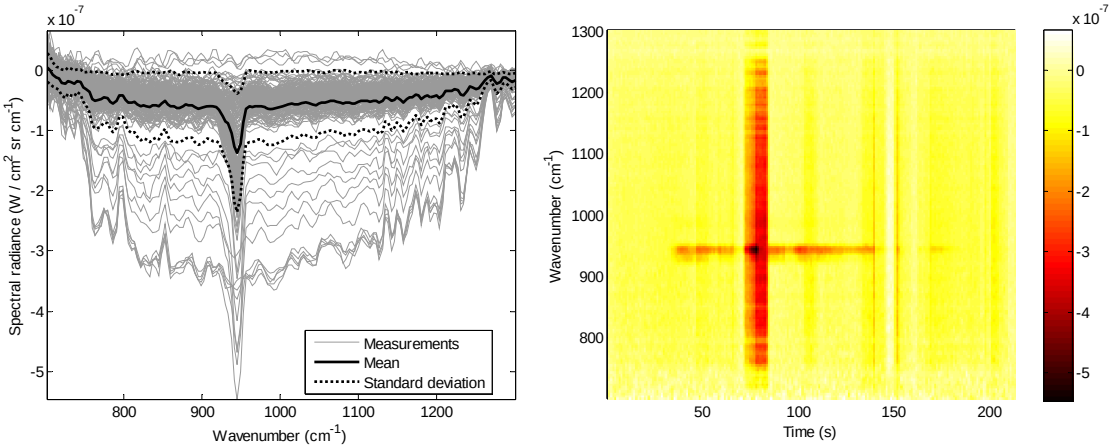

Figure 6: SF_6 release (1.4 kg/min) showing the evolution of the measured differential radiance in different projections; overlay plot of the radiance acquired by CATSI (left) and spectrogram showing the radiance as a function of time (right).

Figure 7 shows the best fit between the SF_6 spectrum computed with the GASEM model (red curve) and the measured differential radiance at 101 s after the beginning of the release. The comparison of the fitted signature and the measured spectrum results in a fit quality of 0.92. This measure of the fit quality gives a degree of confidence in the identification of the released gas.

The bottom part of Figure 7 shows a plot of the goodness of fit (r^2) and the column density (CL) of the SF_6 plume as a function of time determined from the GASEM fitting procedure. The fit was obtained with a filling factor estimated at 90% and the chemical gas temperature was adjusted to the air temperature. The fluctuation in the column density and the goodness of the fit can be attributed to the field of regard (FOR) scanning process, a change in the background temperature or a release fluctuation. The FOR scanning process involves moving the optical head assembly to scan the extent of the chemical plume. It is clearly shown in this figure that CATSI successfully detected and identified the SF_6 plume at a distance of 870 m.

At this distance the FOV was close to 7 m, and from Figure 8 it is evident that the FOV was mostly filled by the release plume assuming the sensor was pointed near the release point. Figure 8 shows the result from a Gaussian plume model that simulates the chemical vapour dissemination as a function of flow rate and wind speed. The result was simulated for an SF_6 release rate of 1.4 kg/min and a wind speed of 3 m/s. In order to verify the CL calculated with the GASEM algorithm, an average value of the CL simulated with the plume model was determined over the CATSI FOV. This resulted in a column density of 220 ppm m, which compares favourably with the measured CL presented in Figure 7.

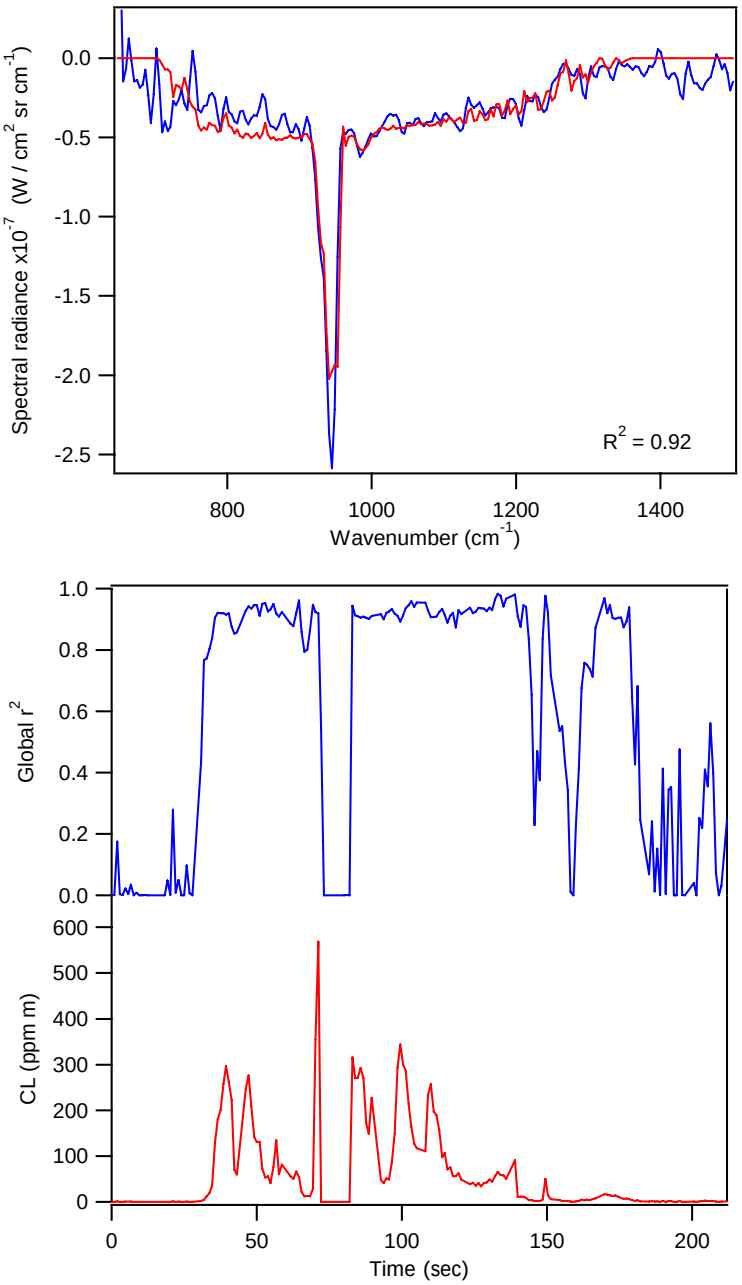

Figure 7: Comparison of the best-fit SF_6 simulation (red curve) with the measured differential radiance spectrum (blue curve) at 188 s after the release began (top). Plot of the goodness of fit (r^2) and the column density (CL) of SF_6 determined from the GASEM fitting procedure (bottom).

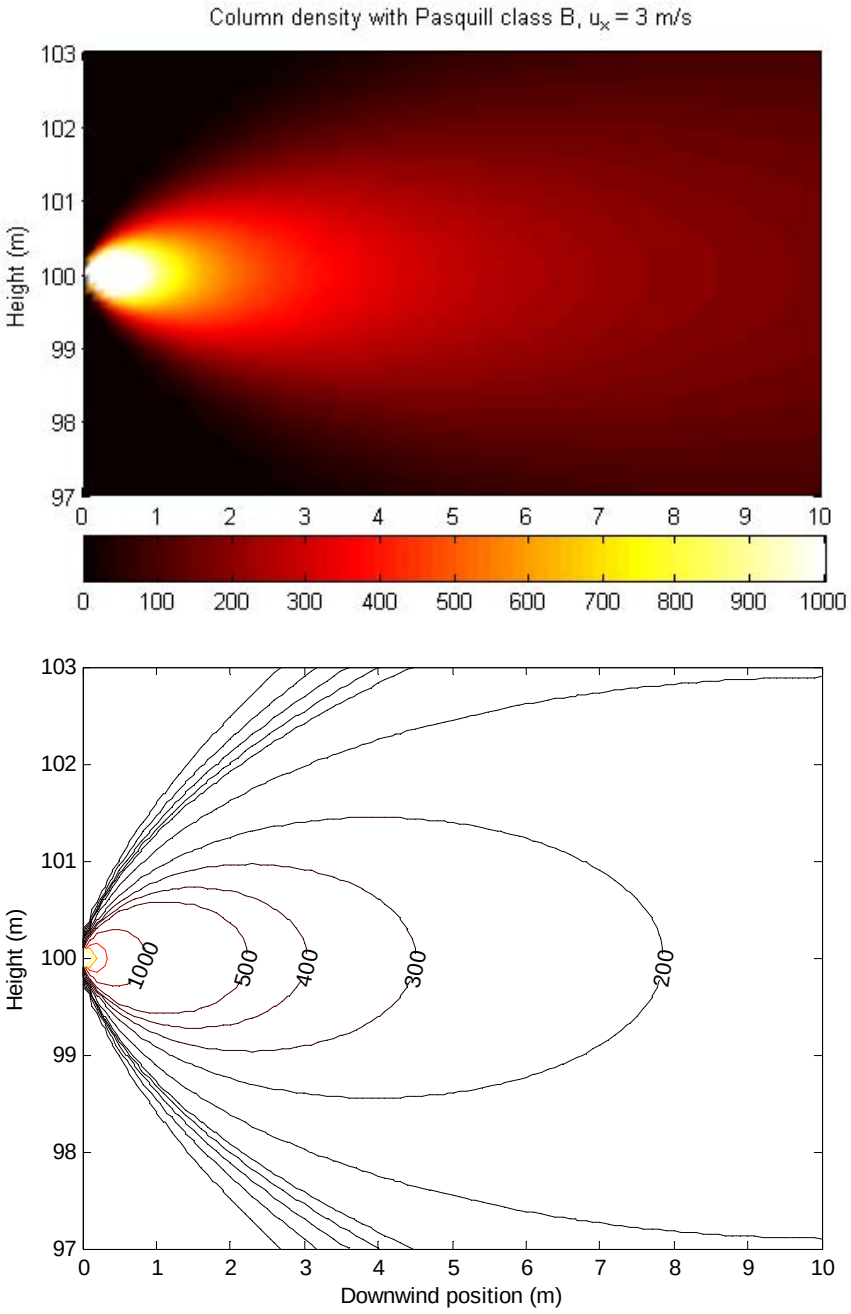

Figure 8: Gaussian plume simulation of SF_6 release at 1.4 kg/min. The lower figure presents the column density (CL in ppm m) as a function of distance.

Figure 9 shows the results obtained for a release of SF_6 at 0.15 kg/min for 5 min at 1440 m from the sensor. The overlay plot and the spectrogram of the differential radiance show all the spectra collected by CATSI during the release, which occurred at 15:26 LT on June 17, 2005. The background for this measurement consisted of a mixture of grass, trees and blue sky. The temperature contrast was evaluated at -0.4 K. The negative sign indicates that the background temperature was lower than the air temperature ($\Delta T = T_{background} - T_{air}$).

The spectrogram in the 940–950 cm^{-1} region shows clearly the evolution of the SF_6 band as a function of time with sufficient SNR to make detection possible in the interval from 100 to 450 s. The red streaks perpendicular to the time axis (150 s, 180 s, 280–320 s) are attributed to intensity fluctuations as shown on the overlay plot. Those streaks can be explained by a change in the background temperature due to clouds moving over the scene or by the scanning procedure where the FOV moves from a hot background to a colder one (sky).

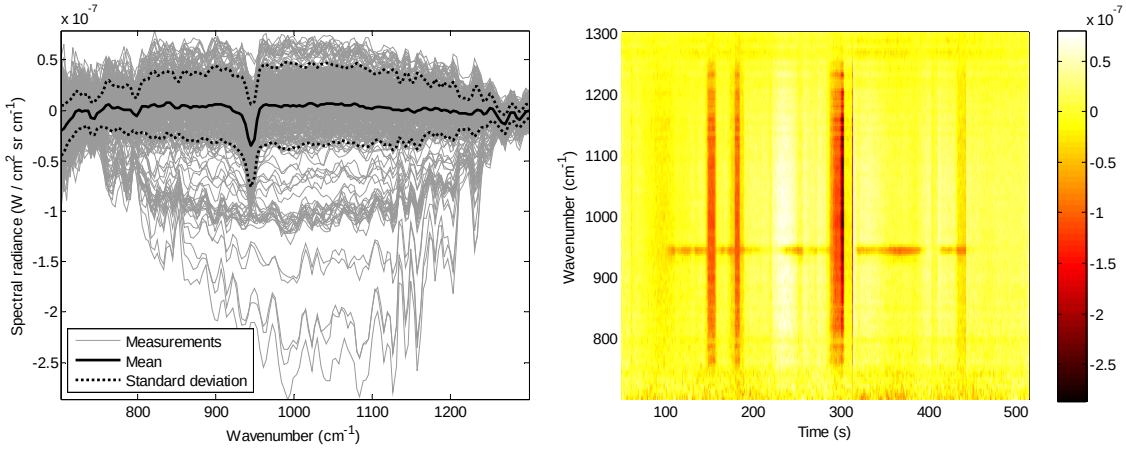

Figure 9: SF_6 release (0.15 kg/min). Evolution of the measured differential radiance in different projections; overlay plot of the radiance acquired by CATSI (left) and spectrogram showing the radiance as a function of time (right).

Figure 10 shows the best fit between the SF_6 spectrum computed with the GASEM model (red curve) and the measured differential radiance at 243 s after the beginning of the release. The comparison of the fitted signature and the measured spectrum results in a fit quality of 0.91. This measure of the fit quality gives a degree of confidence in the identification of the released gas.

The bottom part of Figure 10 shows a plot of the goodness of fit (r^2) and the column density (CL) of SF_6 as a function of time determined from the GASEM fitting procedure. The fit was obtained with a filling factor estimated at 60% and the chemical vapour temperature was adjusted to the air temperature. The fluctuation in the column density and the goodness of the fit can be attributed to the FOR scanning procedure or fast fluctuation of the background temperature.

This figure clearly shows that CATSI detected and identified the SF_6 plume at a distance of 1440 m. The mean CL was estimated at 30 ppm m. This is 7 times less than the result of the previous measurement, which corresponded to a flow rate of 1.4 kg/min (Figure 7). It should be noted that

a comparison of the two flow rates results in a ratio close to ten. Comparison of the temperature contrasts of -0.4 K (associated with a flow rate of 0.15 kg/min) and 1.3 K (associated with a flow rate of 1.4 kg/min for the previous measurement) shows that the difference cannot be merely attributed to the ratio of the flow rates. Since the spectral intensity and the column density are closely related to the temperature contrast, the difference in the ratio could be explained by an error in the ΔT estimation or a radiative saturation for the higher flow rate release and/or also by different wind speeds associated with each of the two releases.

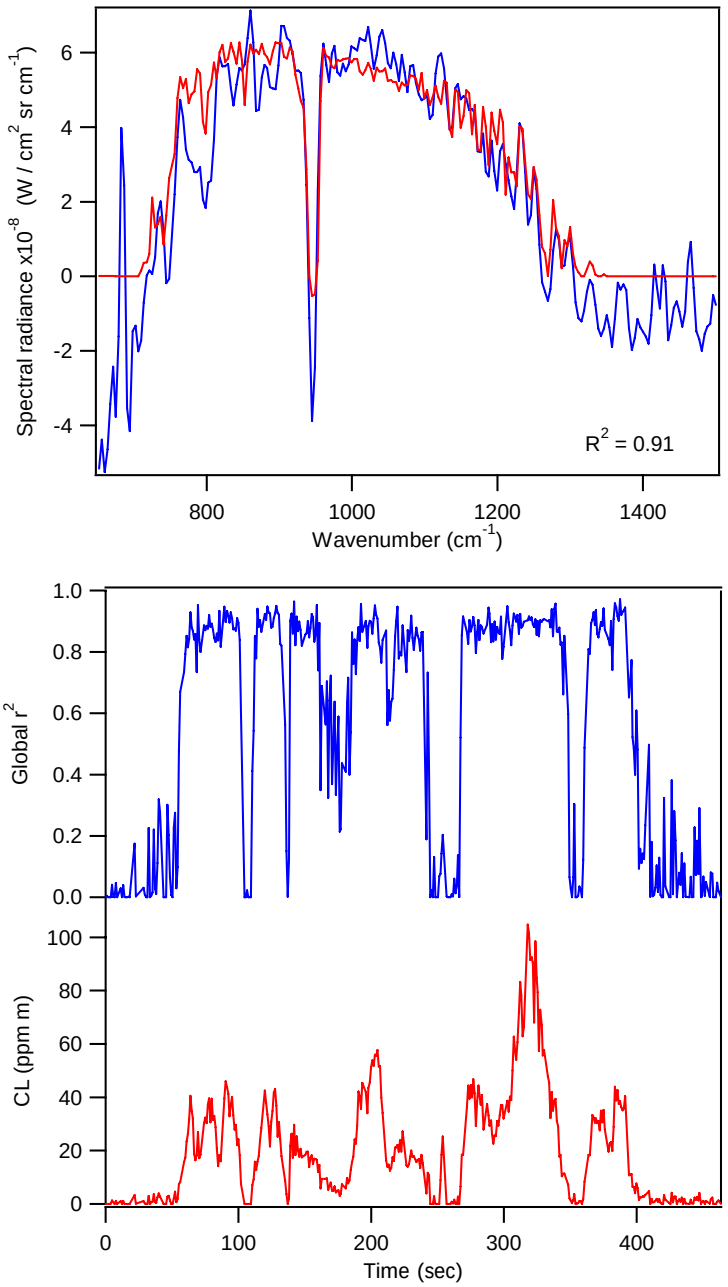

Figure 10: Comparison of the best-fit SF_6 simulation (red curve) with the measured differential radiance spectrum (blue curve) at 243 s after the release began (top). Plot of the goodness of fit (r^2) and the column density (CL) of SF_6 determined from the GASEM fitting procedure (bottom).

At this distance (1440 m) the FOV was close to 11.5 m, and from Figure 8 it is evident that the FOV was mostly filled by the release plume assuming the sensor was pointed near the release point. Figure 11 presents a simulated plume dispersion of SF_6 at 0.15 kg/min and a wind speed of 3 m/s. In order to verify the CL calculated with the GASEM algorithm, an average value of the CL simulated with the plume model was determined over the CATSI FOV. This resulted in a column density of 30 ppm m, which is consistent with the column density obtained from the GASEM fitting procedure presented in Figure 10.

Figure 12 shows spectral simulations performed with GASEM using different column densities of SF_6. The environmental parameters collected by CATSI during the experiment (sec. 4.1.1), including a temperature contrast of 1.3 K, were used for this simulation. It can be observed that the saturation level (maximum absolute intensity) is obtained with a concentration of 100 to 500 ppm m. The simulation also shows that the increase in concentration produces a broadening of the main SF_6 band (945 cm^{-1}) and an increase in the intensity of the second band (990 cm^{-1}).

Comparison of the intensity observed in the measurements (Figure 7 and 10) and the simulation (Figure 12) supports the assumption that the ΔT measured by CATSI is under-evaluated. A more accurate evaluation of the ΔT should result in a better simulation and fit, leading to a more accurate column density of the cloud (see [1]).

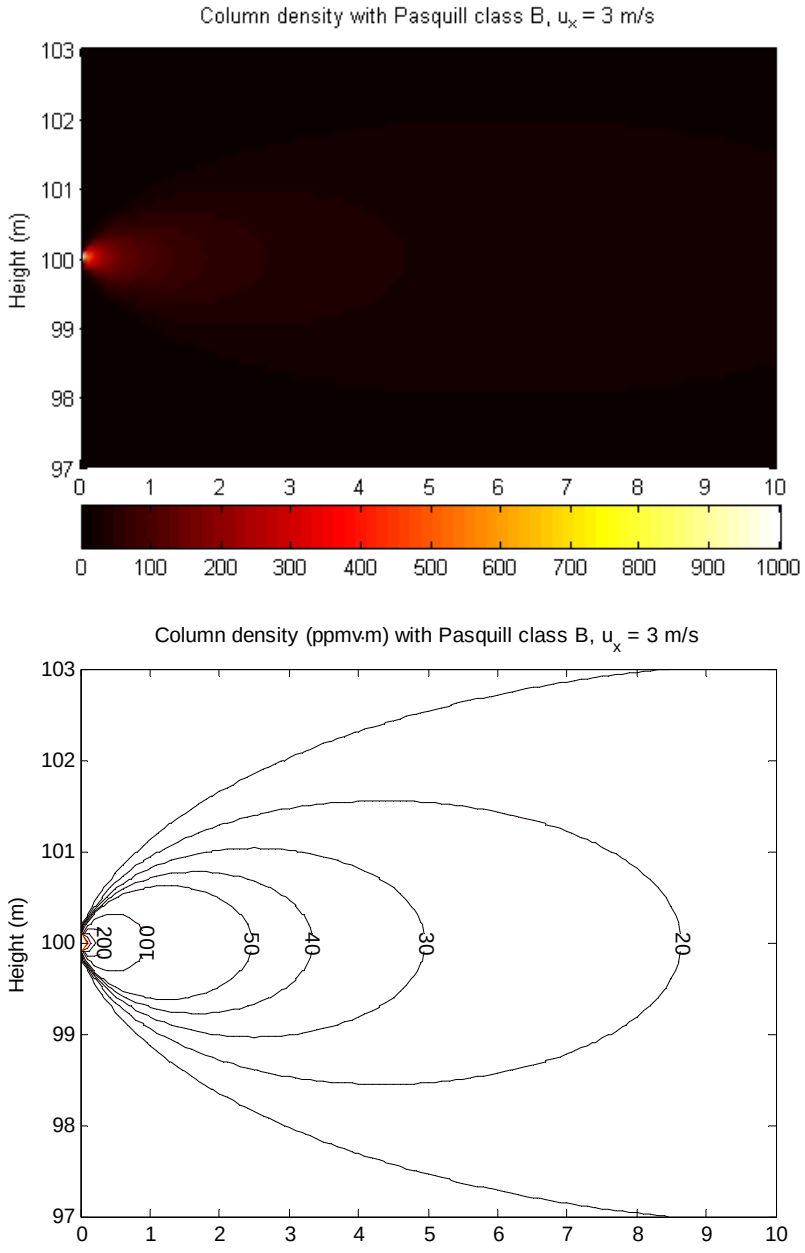

Figure 11: Gaussian plume simulation of SF_6 release at 0.15 kg/min. The lower figure presents the column density (CL in ppm m) as a function of distance.

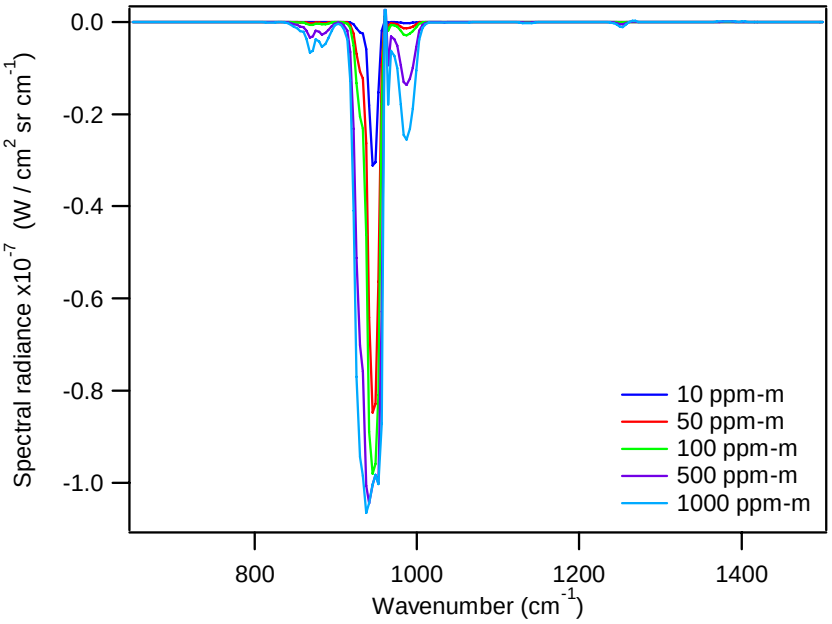

Figure 12: SF_6 differential radiance simulation as a function of column density.

4.1.2 Sulphur hexafluoride and yellow smoke

Figure 13 shows the results obtained for an SF_6 release at 1.25 kg/min for 1 min located 870 m from the sensor and partially masked by yellow smoke. The overlay plot and the spectrogram of the differential radiance show all the spectra collected by CATSI during the release, which occurred at 15:01 LT on June 9, 2005. The background for this measurement consisted mostly of grass, and the temperature contrast was evaluated at 0.5 K. The spectrogram in the 940–950 cm^{-1} region shows clearly the evolution of the SF_6 band over time with a sufficient SNR to permit detection in the interval between 100 and 350 s.

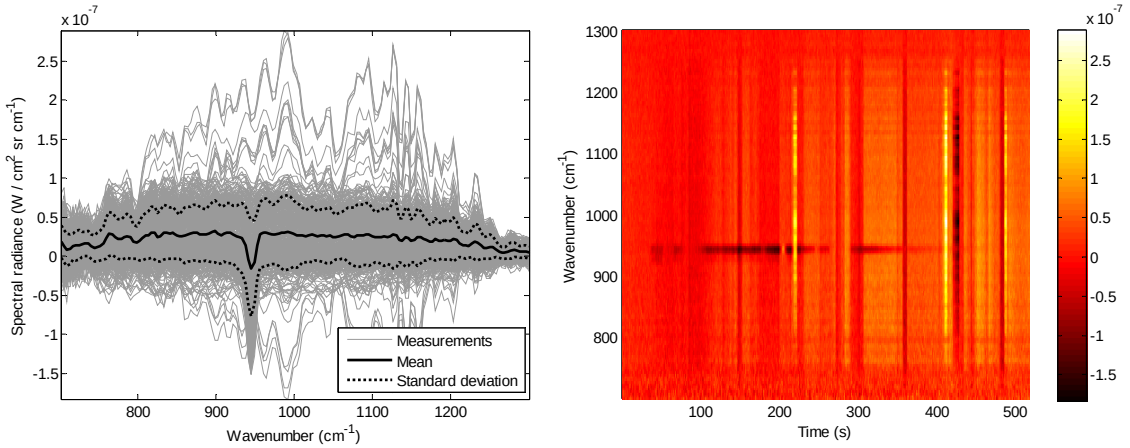

Figure 13: SF_6 release (1.25 kg/min) partially masked by yellow smoke. Evolution of the measured differential radiance in different projections; overlay plot of the radiance acquired by CATSI (left) and a spectrogram showing the radiance as a function of time (right).

Figure 14 shows the best fit between the SF_6 spectrum computed with the GASEM model (red curve) and the measured differential radiance at 210 s after the release began. The comparison of the fitted signature with the measured spectrum gives a fit quality of 0.90. The bottom part of Figure 14 shows a plot of the goodness of fit (r^2) and the column density (CL) of SF_6 as a function of time determined from the GASEM fitting procedure. The fit was obtained with a filling factor estimated at 90% and the chemical gas temperature was adjusted to the air temperature. The fluctuation in the column density and the goodness of the fit can be attributed to the FOR scanning procedure. This figure clearly shows that CATSI detected and identified the SF_6 plume at a distance of 870 m in the presence of yellow smoke released as an obscurant. The smoke had no significant effect on the detection and identification procedure.

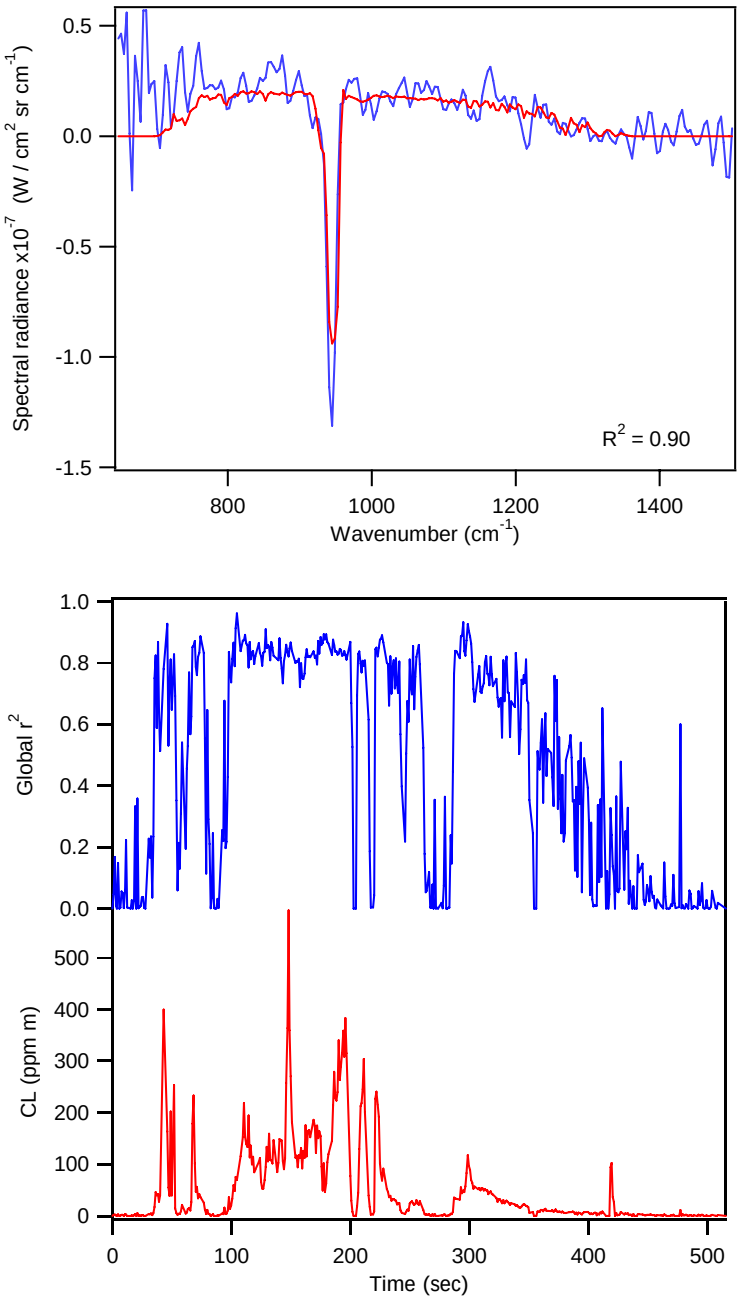

Figure 14: Comparison of the best-fit SF_6 simulation (red curve) with the measured differential radiance spectrum (blue curve) at 210 s after the release began (top). Plot of the goodness of fit (r^2) and the column density (CL) of SF_6 determined from the GASEM fitting procedure (bottom).

An analysis of the measurement evolution graphs (Figure 6, 9 and 13) shows fluctuations over time. These fluctuations are attributed to a change in the background radiance relative to the radiance acquired by the sensor during the calibration. This radiance fluctuation could affect the effective ΔT as a function of time. These fluctuations can also be attributed to the scene scanning process where the sensor head is moved to scan the extent of the chemical vapour, resulting in measured changes in vapour concentration and background radiance. Clouds higher up in the atmosphere may also introduce shadowing effects that can change the temperature of the background scene or chemical vapour.

A comparison of the differential radiances obtained for the three SF_6 measurements (top views of Figure 7, 10 and 14) shows that the evaluation of the ΔT is very important for the column density determination. The differential spectral radiance between the baseline and the maximum in the SF_6 intensity are approximately 1.7, 1.0 and 1.5 x 10^{-7} W / (cm sr cm^{-1}) for the measurements performed at flow rates of 1.4 (Figure 7), 0.15 (Figure 10) and 1.25 (Figure 14) kg/min, respectively.

The analysis of the column densities obtained with GASEM for SF_6 releases with and without yellow smoke obscurant (Figure 7 and 14) shows that the results are similar. This result provides evidence that this type of obscurant can degrade the level of detection or the radiance intensity measured by the sensor, but the LWIR passive system is still able to detect and identify the chemical released. Despite the fact that yellow smoke is not a common battlefield obscurant, it is possible that other obscurants that have no spectral signature could give results similar to those shown here. This kind of obscurant decreases the detectability of a chemical vapour but it will not interfere with the identification process, since the obscurant causes no chemical change in the gas. Conversely, an obscurant with a signature could interfere with the identification process by masking or modifying part of the chemical vapour signature. This result is an important first step in assessing the impact of obscurants on chemical releases; however, many more experiments are needed before any definite conclusions can be established.

4.1.3 Ammonia (NH_3)

Figure 15 shows the results obtained for a release of NH_3 at 0.825 kg/min for 2 min at 870 m from the sensor. The overlay plot and the spectrogram of the differential radiance show all the spectra collected by CATSI during the release time at 15:18 LT on June 9, 2005. The background for this measurement consisted mostly of grass, and the temperature contrast was evaluated at -0.1 K. The spectrogram in the 900–1000 cm^{-1} region shows clearly the evolution of the NH_3 bands over time with a sufficient SNR to enable detection in the interval between 25 and 150 s. The fluctuation observed in the spectrogram is the result of the scene scanning process, which determines whether or not ammonia is present in the FOV.

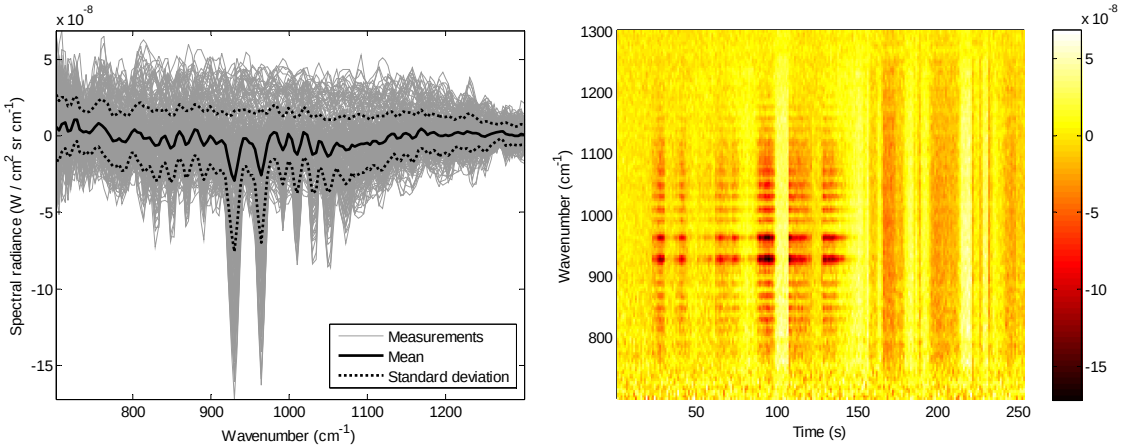

Figure 15: Ammonia release (0.825 kg/min). Evolution of the measured differential radiance in different projections; overlay plot of the radiance acquired by CATSI (left), and spectrogram showing the radiance as a function of time (right).

Figure 16 shows the best fit between the NH_3 spectrum computed with the GASEM model (red curve) and the measured differential radiance at 93 s after the release started. The comparison of the fitted signature and the collected spectrum gives a fit quality of 0.85. The bottom part of Figure 16 shows a plot of the goodness of fit (r^2) and the column density (CL) of NH_3 as a function of time determined from the GASEM fitting procedure. The fit was obtained with a filling factor estimated at 90% and the chemical gas temperature was adjusted to the air temperature. The fluctuation in the column density and the goodness of the fit can be attributed to the FOR scanning procedure.

Figure 17 represents a plume dispersion of NH_3 at 0.825 kg/min and a wind speed of 3 m/s. At this distance (870m) the FOV is approximately 7 m, and using the results of the plume model in Figure 17, it is apparent that the FOV is mostly filled by the release plume if the sensor is pointed close to the release point. To verify the CL estimated with the GASEM algorithm, an average over the CATSI FOV was calculated to extract the CL from the simulation in Figure 17. For this measurement, a column density of 1900 ppm m was calculated and it compares favourably with the measured CL presented in Figure 16.

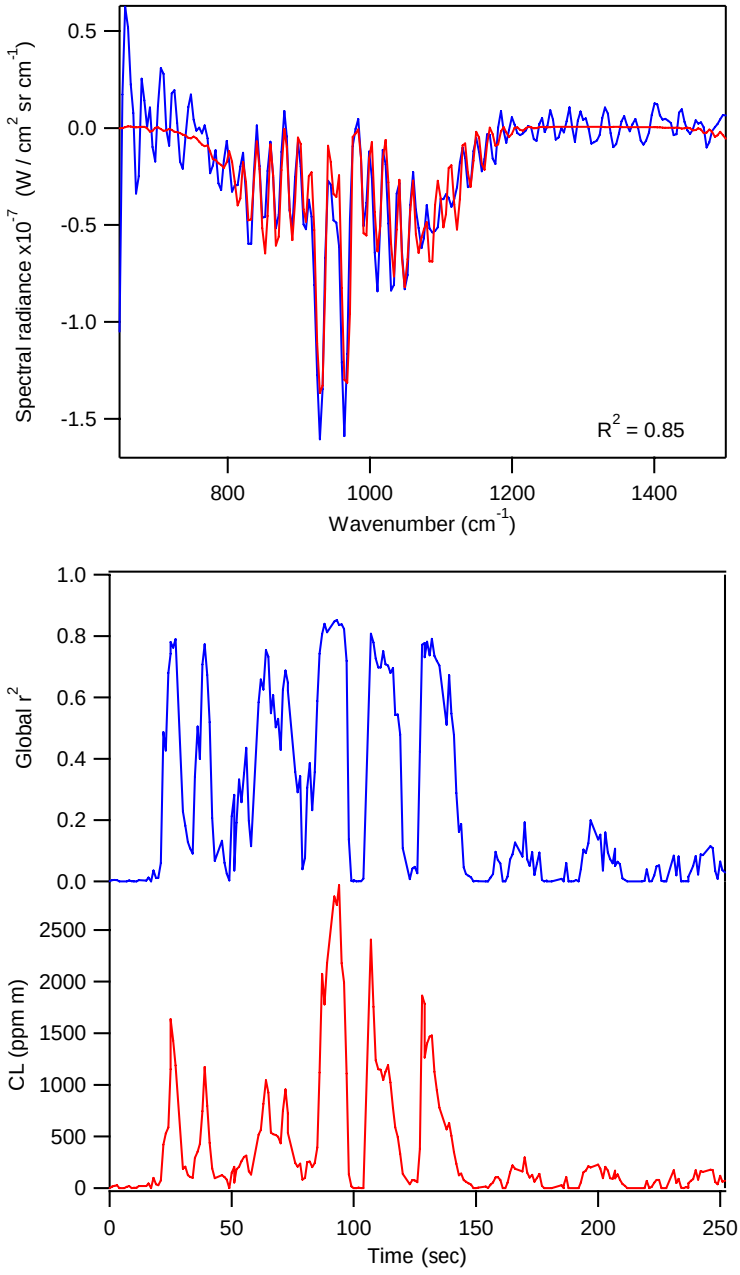

Figure 16: Comparison of the best-fit NH_3 simulation (red curve) with the measured differential radiance spectrum (blue curve) at 93 s after the start of the release (top). Plot of the goodness of fit (r^2) and the column density (CL) of NH_3 determined from the GASEM fitting procedure (bottom).

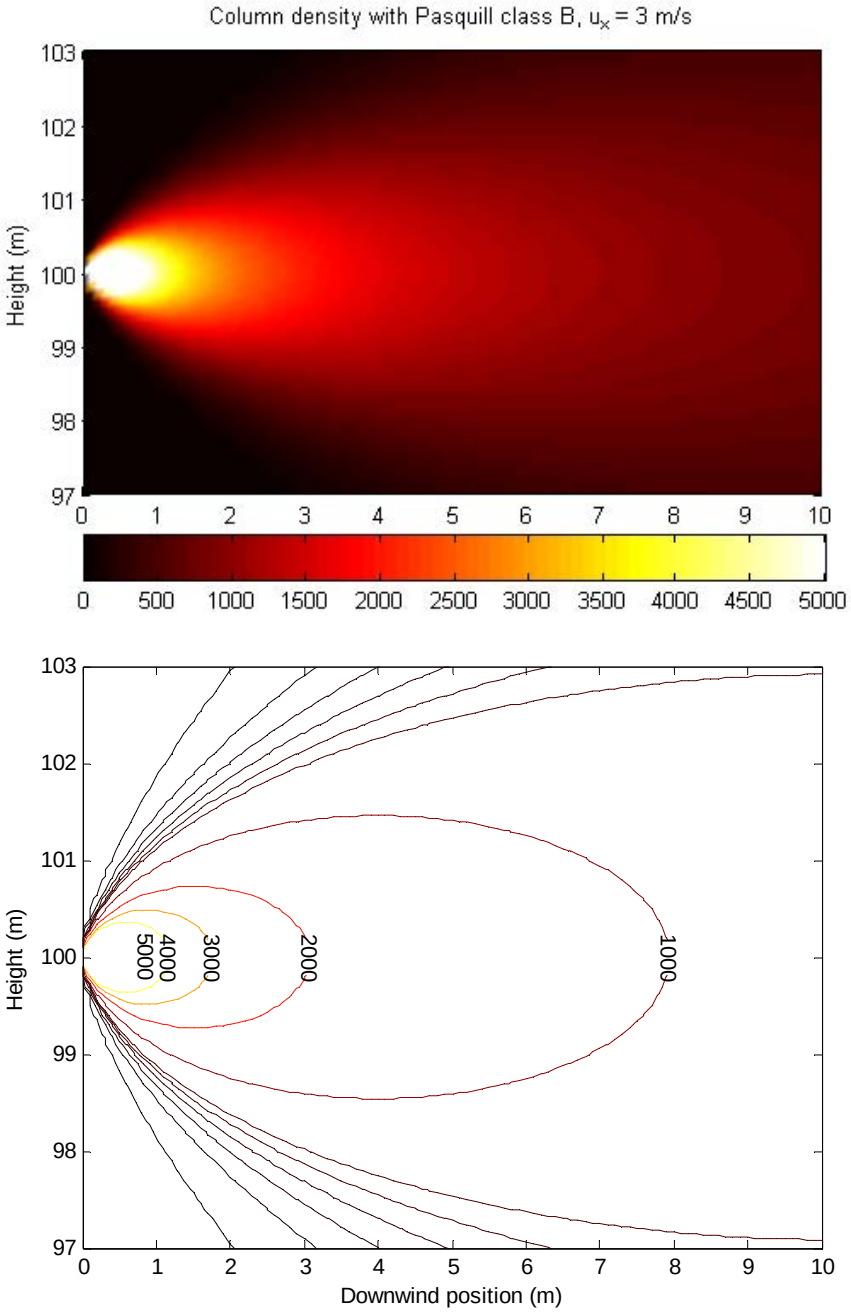

Figure 17: Gaussian plume simulation of an NH_3 release at 0.825 kg/min. The lower figure presents the column density (CL in ppm m) as a function of distance.

4.1.4 Ammonia and yellow smoke

Figure 18 shows the results obtained for a release of NH_3 at 0.8 kg/min for 2 min located 870 m from the sensor and partially masked by yellow smoke. The overlay plot and the spectrogram of the differential radiance show all the spectra collected by CATSI during the release time, which was 15:24 LT on June 9, 2005. The background for this measurement consisted mostly of grass, and the temperature contrast was evaluated to be approximately 0 K. This ΔT is not consistent with the measured results and this demonstrates a limitation in the ΔT determination process. The spectrogram in the 900–1000 cm^{-1} region shows clearly the evolution of the NH_3 bands over time, with a sufficient SNR to permit detection in the interval between 40 and 300 s.

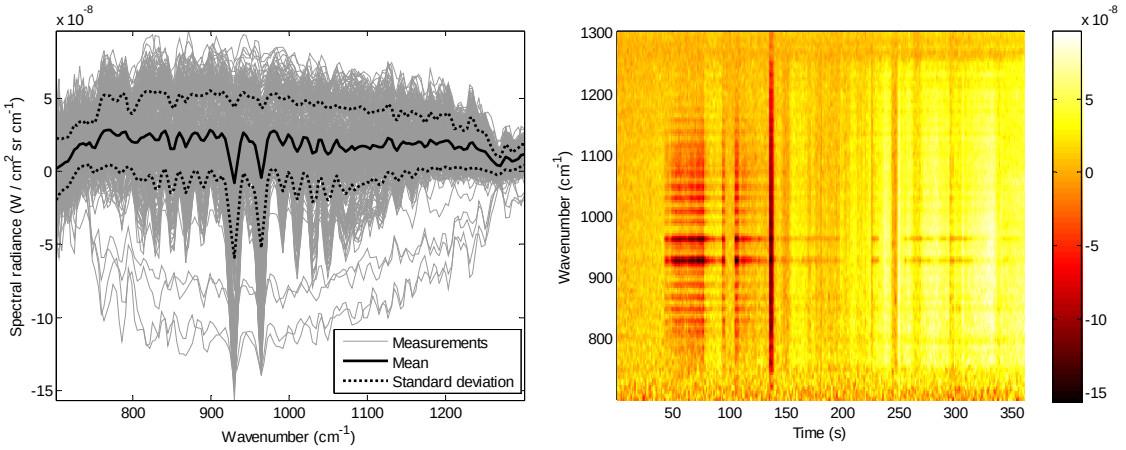

Figure 18: Ammonia release (0.8 kg/min) masked by yellow smoke. Evolution of the measured differential radiance in different projections; overlay plot of the radiance acquired by CATSI (left), and spectrogram showing the radiance as a function of time (right).

Figure 19 shows the best fit between the NH_3 spectrum computed with the GASEM model (red curve) and the measured differential radiance at 73 s after the start of the release. The comparison of the fitted signature and the measured spectrum gives a fit quality of 0.80. The bottom part of Figure 19 shows a plot of the goodness of fit (r^2) and the column density (CL) of NH_3 as a function of time determined from the GASEM fitting procedure. The fit was obtained with a filling factor estimated at 90% and the chemical gas temperature was adjusted to the air temperature. The fluctuation in the column density and the goodness of the fit can be attributed to the FOR scanning procedure. Typically, the fit quality is greater than 0.75 when the gas cloud is present in the field of view. This figure clearly shows that CATSI detected and identified the NH_3 plume at a distance of 870 m in the presence of yellow smoke. The comparison between Figure 15 and 18 shows a similar spectral intensity with a very small temperature contrast difference. As in the release of SF_6 with smoke, the yellow smoke released as an obscurant with ammonia had only a small effect on the detection and identification procedure.

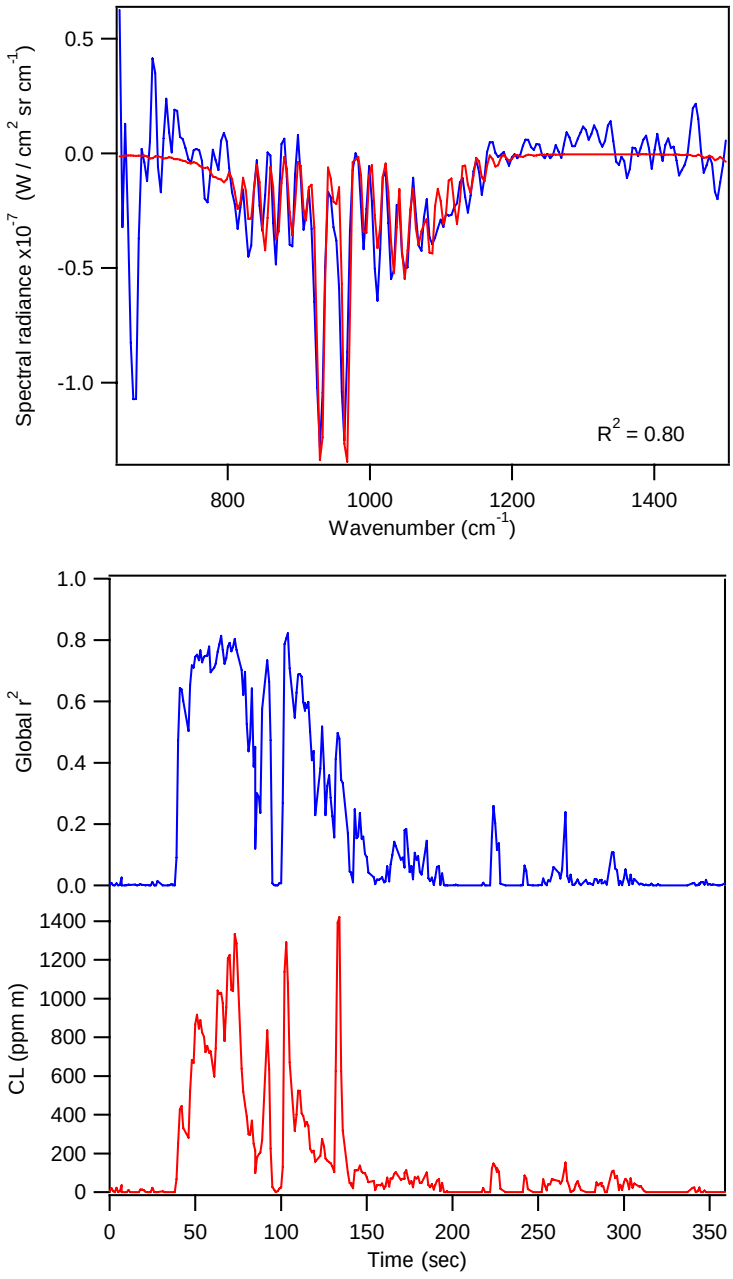

Figure 19: Comparison of the best-fit NH_3 simulation (red curve) with the measured differential radiance spectrum (blue curve) at 73 s after the release began (top). Plot of the goodness of fit (r^2) and the column density (CL) of NH_3 determined from the GASEM fitting procedure (bottom).

4.1.5 Mixture of SF_6 and NH_3

Figure 20 shows the results obtained for a mixed release of SF_6 and NH_3 at 0.975 and 0.75 kg/min, respectively, for 2 min at 870 m from the sensor. The overlay plot and the spectrogram of the differential radiance show all the spectra collected by CATSI during the release time, which was 15:55 LT on June 9, 2005. The background for this measurement consisted mostly of grass, and the temperature contrast was evaluated at 0.3 K. The spectrogram in the 900–1000 cm^{-1} region shows clearly the evolution of the combined SF_6 and NH_3 bands over time, and with sufficient SNR to permit detection in the interval between 30 and 300 s.

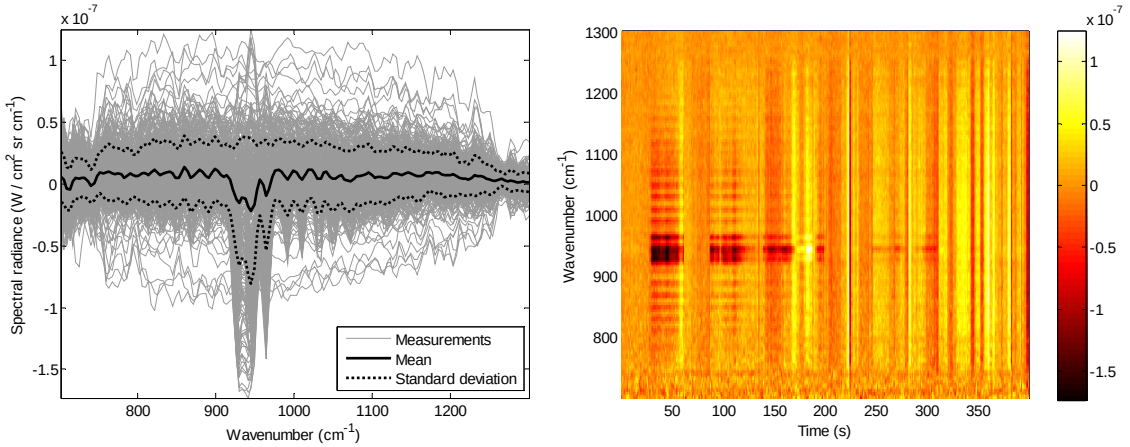

Figure 20: SF_6 and NH_3 mixture release (0.975 and 0.75 kg/min respectively). Evolution of the measured differential radiance in different projections; overlay plot of the radiance acquired by CATSI (left), and spectrogram showing the radiance as a function of time (right).

Figure 21 shows the best fit between the SF_6-NH_3 spectrum computed with the GASEM model (red curve) and the measured differential radiance at 103 s after the release began. The comparison of the fitted signature and the measured spectrum give a fit quality of 0.83. The bottom part of Figure 21 shows a plot of the goodness of fit (r^2) and the column density (CL) of SF_6 and NH_3 as a function of time determined from the GASEM fitting procedure. The fit was obtained with a filling factor estimated at 90% and the chemical gas temperature was adjusted 0.7 K lower than the air temperature to permit a better fit. The fluctuation in the column density and the goodness of the fit can be attributed to the FOR scanning procedure. The quality of fit is greater than approximately 0.80 when the gas cloud is present in the field of view, and this figure clearly shows that CATSI detected and identified the SF_6-NH_3 mixed plume at a distance of 870 m.

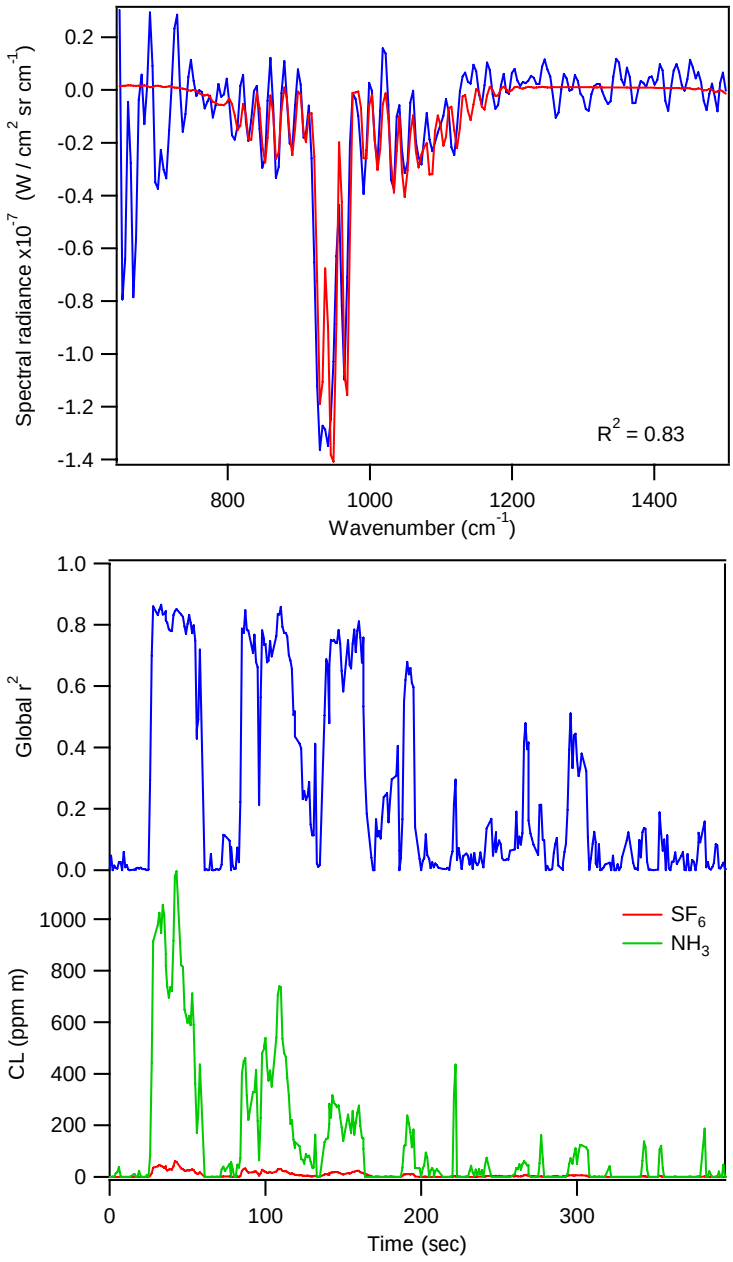

Figure 21: Comparison of the best-fit SF_6 and NH_3 mixture simulation (red curve) with the measured differential radiance spectrum (blue curve) at 103 s after the release began (top). Plot of the goodness of fit (r^2) and the column density (CL) of SF_6 and NH_3 determined from the GASEM fitting procedure (bottom).

4.2 CWA simulant (liquid)

Liquid simulants DMMP and TEP were released to challenge the passive LWIR sensors in detecting and identifying materials characterized by a lower vapour pressure. The liquids were released by spraying to form a plume, and the resulting small droplets evaporated and formed a vapour cloud of DMMP or TEP.

4.2.1 Pure DMMP

Figure 22 shows the results obtained for a release of DMMP at 0.5 kg/min for 1 min at 645 m from the sensor. The overlay plot and the spectrogram of the differential radiance show all the spectra collected by CATSI during the release time, which was 12:29 LT on June 21, 2005. The background for this measurement consisted primarily of grass, and the temperature contrast was evaluated at approximately 0.5 K. The spectrogram in the 1000–1100 cm^{-1} region clearly shows the evolution of the DMMP band over time with a sufficient SNR to enable detection of the gas in the interval between 90 and 150 s.

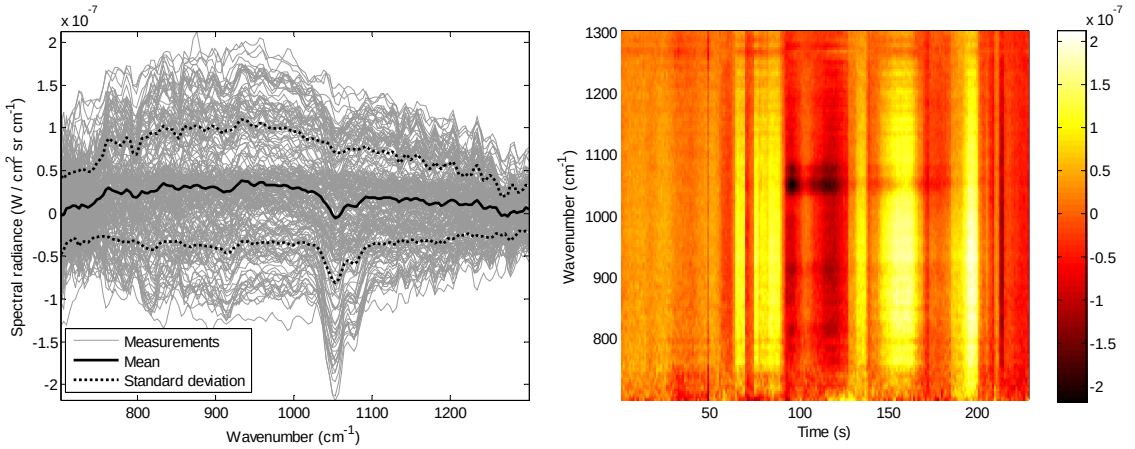

Figure 22: DMMP release (0.5 kg/min). Evolution of the measured differential radiance in different projections; overlay plot of the radiance acquired by CATSI (left), and spectrogram showing the radiance as a function of time (right).

Figure 23 shows the best fit between the DMMP spectrum computed with the GASEM model (red curve) and the measured differential radiance at 96 s after the release began. The comparison of the fitted signature with the measured spectrum gives a fit quality of 0.90. The bottom part of Figure 23 shows a plot of the goodness of fit (r^2) and the column density (CL) of DMMP vapour as a function of time determined from the GASEM fitting procedure. The fit was obtained with a filling factor estimated at 90% and the chemical gas temperature was adjusted 1.5 K lower than the air temperature in order to obtain a better fit. The fluctuation in the column density and the goodness of the fit can be attributed to the FOR scanning procedure. The quality of fit is greater than approximately 0.80 when the gas cloud is present in the field of view, and this figure clearly shows that CATSI detected and identified the DMMP vapour plume at a distance of 645 m.

Several measurements were performed during the experiment where the FOV was centred on the release nozzle to look directly at the liquid phase; however, no DMMP features were detected within the measured SNR of the spectra.

At this distance (645m) the FOV was approximately 5 m, and from Figure 24 it is evident that the FOV was mostly filled by the release plume if the sensor was pointed near the release point. Figure 24 presents a plume dispersion of DMMP at 0.5 kg/min and a wind speed of 3 m/s. To verify the CL value calculated with the GASEM algorithm, an average CL value was calculated over the CATSI FOV from the plume simulation. For this simulation, a column density of 180 ppm m was calculated and it can be compared with the measured CL presented in Figure 23. The comparison shows that the measured CL is 2 to 3 times less than that derived from the plume model. However, the DMMP was released in liquid phase and the liquid aerosol plume was still visible 1 to 2 m from the release point. Hence, an appreciable amount of DMMP remained in the liquid phase, which was not detectable by the sensor, leading to an overestimation of the amount of gas simulated with the plume model.

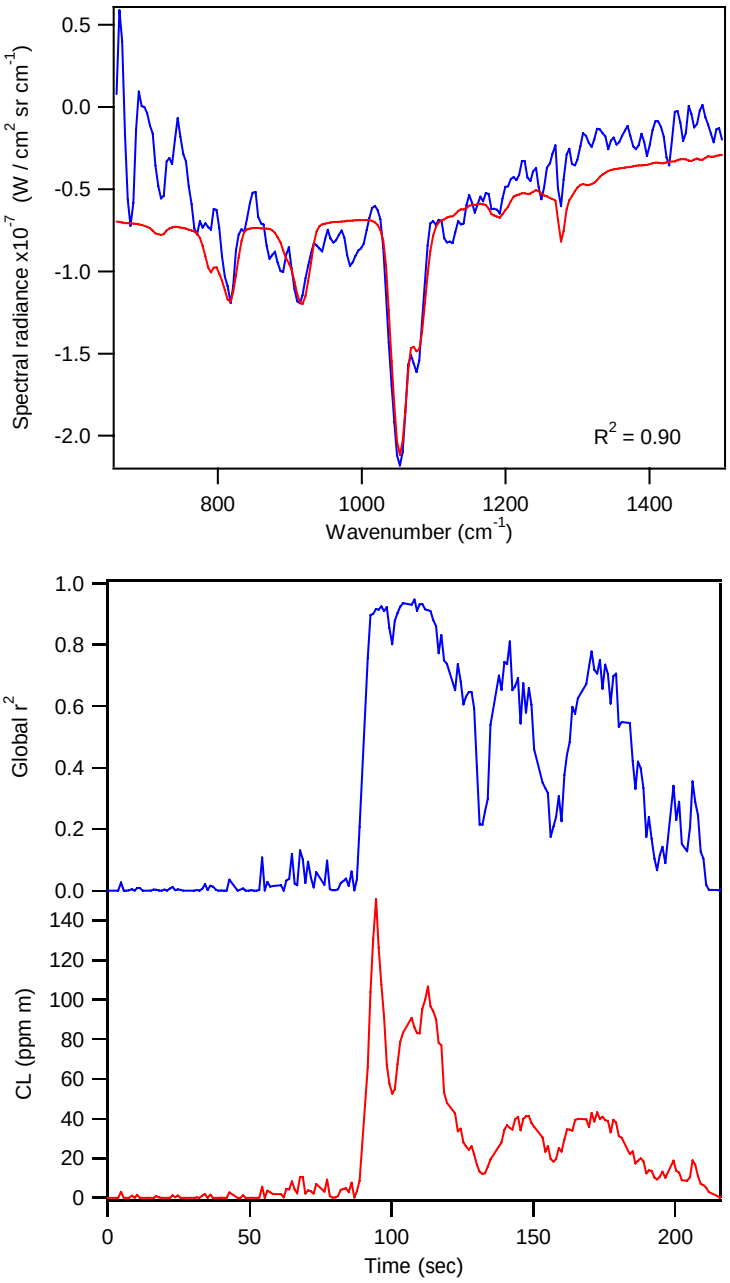

Figure 23: Comparison of the best-fit DMMP simulation (red curve) with the measured differential radiance spectrum (blue curve) at 96 s after the release began (top). Plot of the goodness of fit (r^2) and the column density (CL) of DMMP determined from the GASEM fitting procedure (bottom).

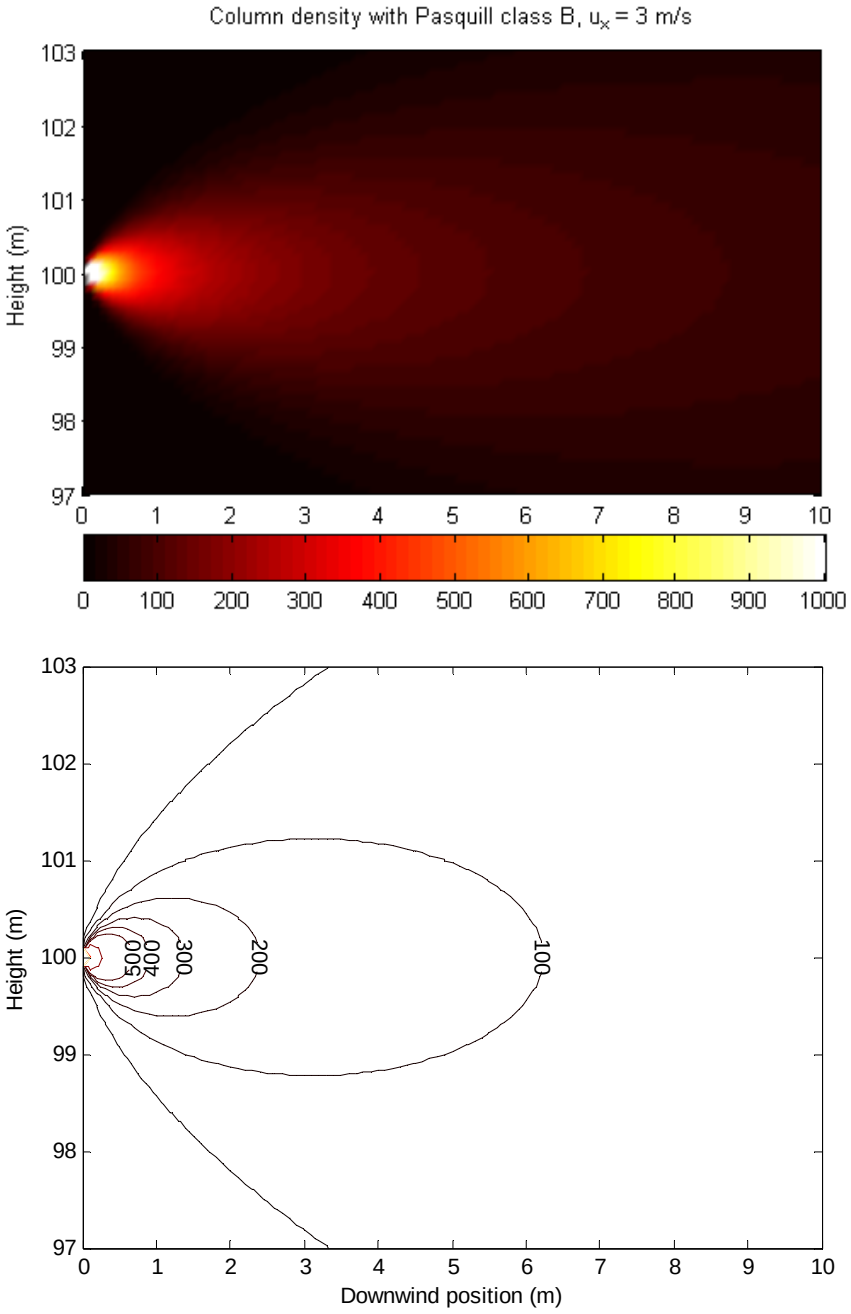

Figure 24: Gaussian plume simulation of a DMMP release at 0.5 kg/min. The lower figure presents the column density (CL in ppm m) as a function of distance.

4.2.2 Pure TEP

Figure 25 shows the results obtained for a release of TEP at 0.6 kg/min for 1 min at a distance of 635 m from the sensor. The overlay plot and the spectrogram of the differential radiance show all the spectra collected by CATSI during the release, which occurred at 15:35 LT on June 21, 2005. The background for this measurement consisted mostly of grass, and the temperature contrast was evaluated at approximately 0.1 K. The spectrogram in the 1000–1100 cm^{-1} region clearly shows the evolution of the TEP band over time with a sufficient SNR to permit detection of the gas in the interval between 120 and 160 s.

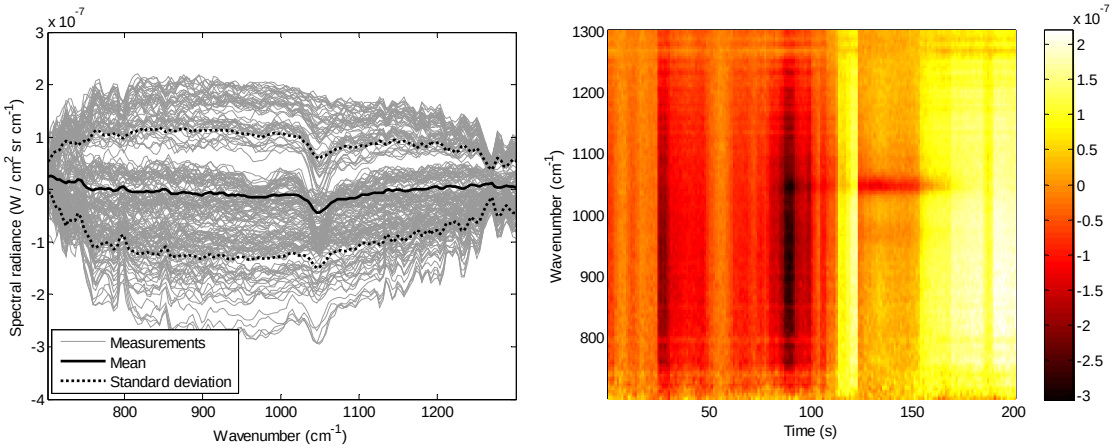

Figure 25: TEP release (0.6 kg/min). Evolution of the measured differential radiance in different projections; overlay plot of the radiance acquired by CATSI (left) and spectrogram showing the radiance as a function of time (right).

Figure 26 shows the best fit between the TEP spectrum computed with the GASEM model (red curve) and the measured differential radiance at 131 s after the release began. The comparison of the fitted signature and the measured spectrum results in a fit quality of 0.94. The bottom part of Figure 26 shows a plot of the goodness of fit (r^2) and the column density (CL) of TEP vapour as a function of time determined from the GASEM fitting procedure. The fit was obtained with a filling factor estimated at 90% and the chemical gas temperature was adjusted 1.5 K lower than the air temperature to obtain the best fit. The fluctuation in the column density and the goodness of the fit can be attributed to the FOR scanning procedure.

The SNR for these measurements was sufficient to permit a clear detection and identification of TEP with a fit quality of about 0.85 when the gas cloud was present within the FOV. This clearly illustrates that CATSI can detect and identify TEP vapours at a distance of 635 m.

At this distance the FOV was approximately 5 m, and from Figure 27 it is evident that the FOV was mostly filled by the release plume if the sensor was pointed near the release point. Figure 27 presents a plume dispersion of TEP at 0.6 kg/min and a wind speed of 3 m/s. In order to verify the CL value calculated with the GASEM algorithm, an average CL value was calculated over the CATSI FOV from the plume simulation. For this simulation, a column density of 140 ppm m was

calculated and it can be compared with the measured CL presented in Figure 26. The comparison shows that the measured CL is 2 to 3 times less than that derived from the plume model. However, the TEP was released in liquid phase and the liquid aerosol plume was still visible 1 to 2 m from the release point. As before, several measurements were performed of the liquid phase located near the release nozzle; however, no TEP spectrum was observed. Hence, an appreciable amount of TEP remained in the liquid phase, which was not detectable by the sensor, leading to an overestimation of the amount of gas simulated with the plume model.

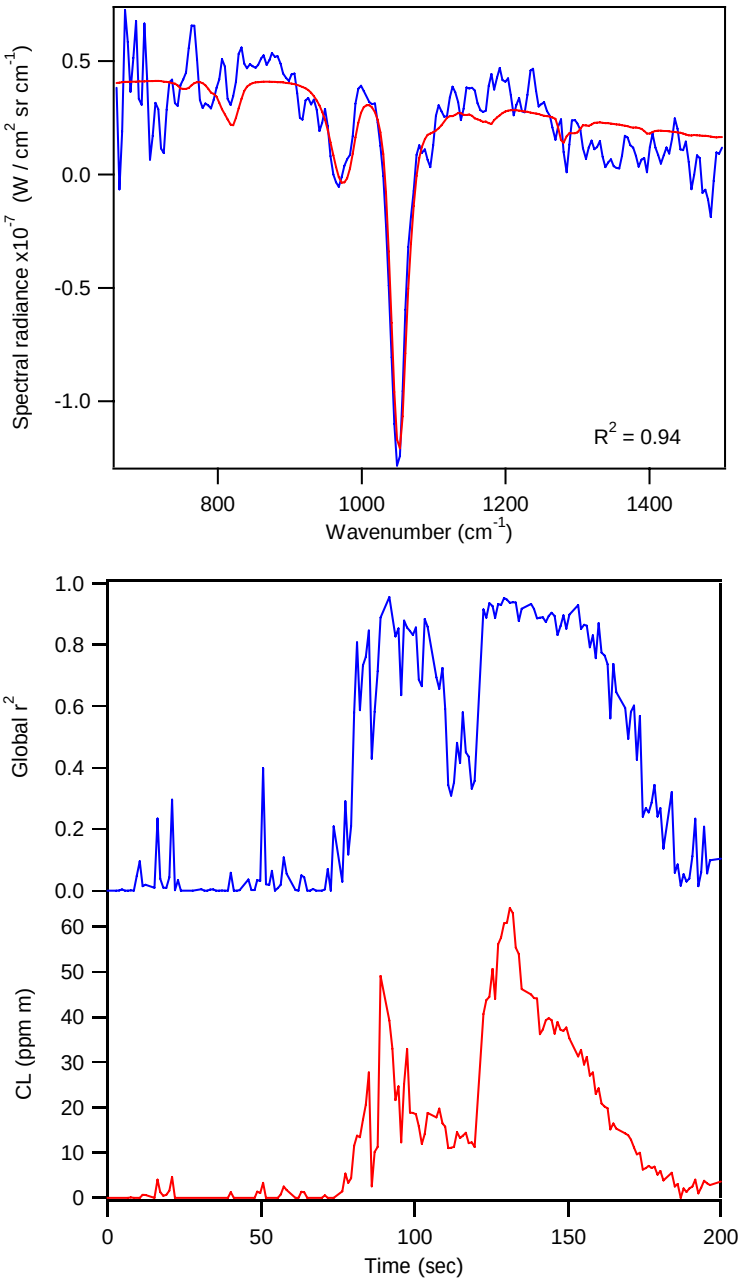

Figure 26: Comparison of the best-fit TEP simulation (red curve) with the measured differential radiance spectrum (blue curve) at 132 s after the release began (top). Plot of the goodness of fit (r^2) and the column density (CL) of TEP determined from the GASEM fitting procedure (bottom).

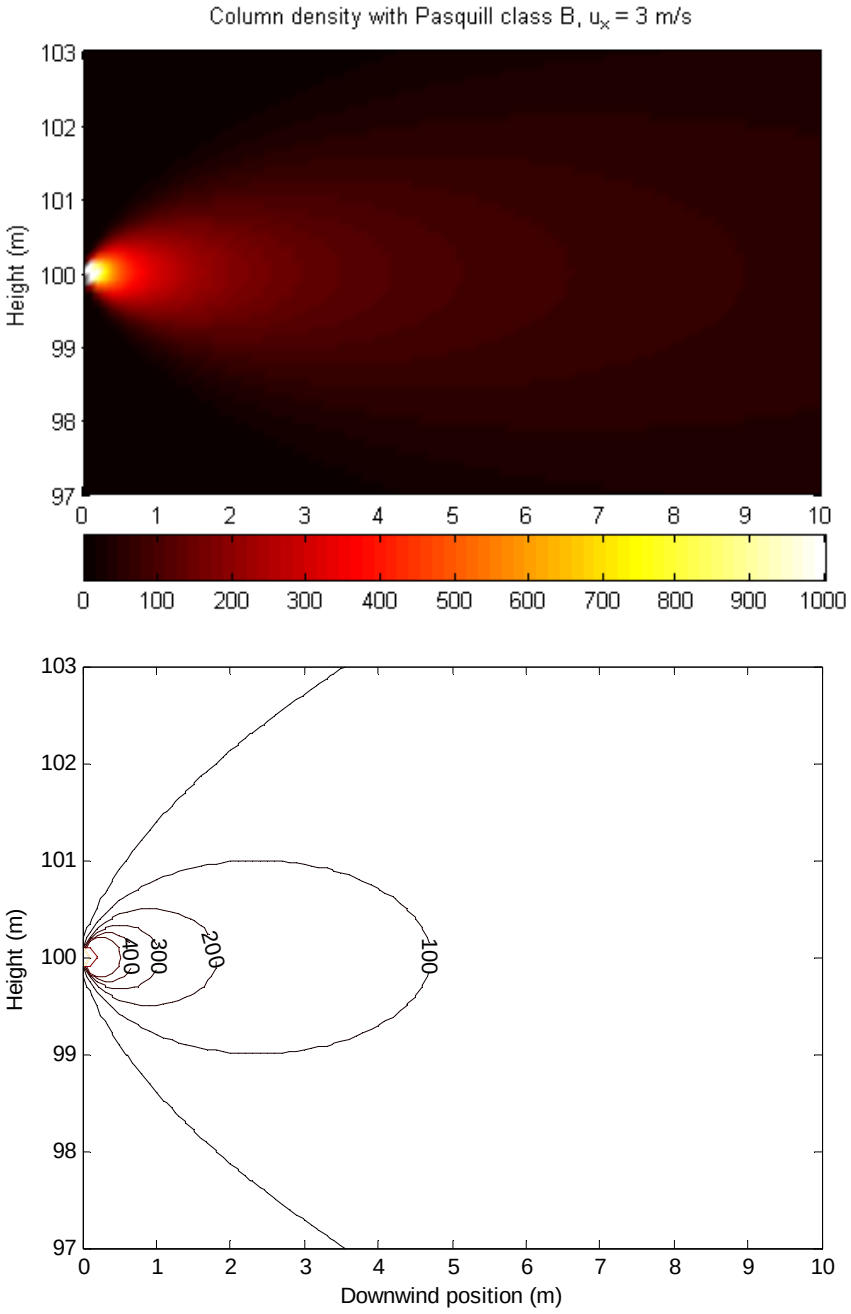

Figure 27: Gaussian plume simulation of a TEP release at 0.6 kg/min. The lower figure presents the column density (CL in ppm m) as a function of distance.

4.2.3 Mixture of DMMP and TEP

Figure 28 shows the results obtained for a mixed release of DMMP and TEP at a rate of 1 kg/min each for 1 min at 1515 m from the sensor. The overlay plot and the spectrogram of the differential radiance show all spectra collected by CATSI during the release time, which was 15:49 LT on June 27, 2005. The background for this measurement consisted mostly of grass, and the temperature contrast was evaluated at -0.2 K. The spectrogram in the 1000–1100 cm^{-1} region clearly shows the evolution of the DMMP and TEP bands over time with a sufficient SNR to permit detection of the mixture in the interval between 60 and 110 s.

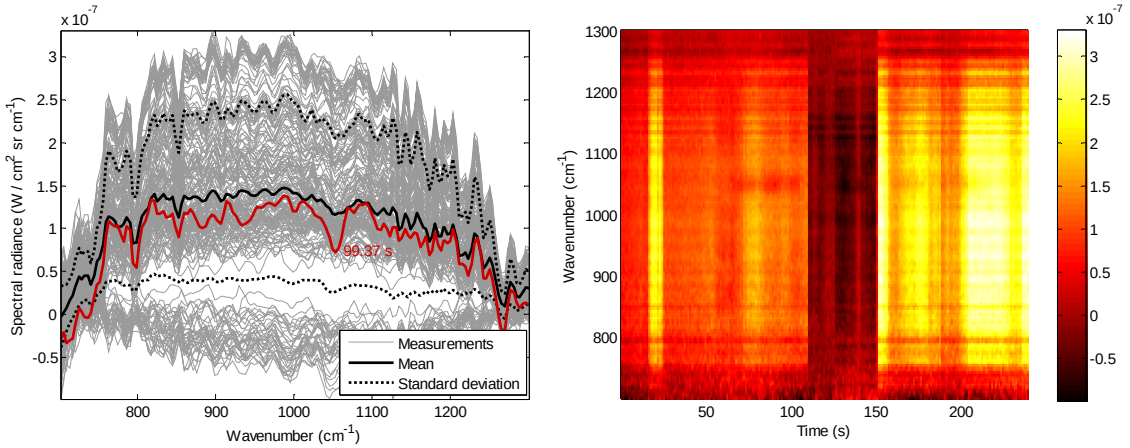

Figure 28: DMMP and TEP mixture release (1.0 kg/min each). Evolution of the measured differential radiance in different projections; overlay plot of the radiance acquired by CATSI (left), and spectrogram showing the radiance as a function of time (right).

Figure 29 shows the best fit between the DMMP-TEP spectrum computed with the GASEM model (red curve) and the measured differential radiance at 88 s (top) and 131 s (bottom) after the release began. The comparison of the fitted signatures and measured spectra results in a fit quality of 0.91 and 0.92. The top graph of Figure 29 shows a best fit where the vapour detected can be identified as mostly composed of TEP. In the bottom graph of Figure 29 the vapour is mostly DMMP.

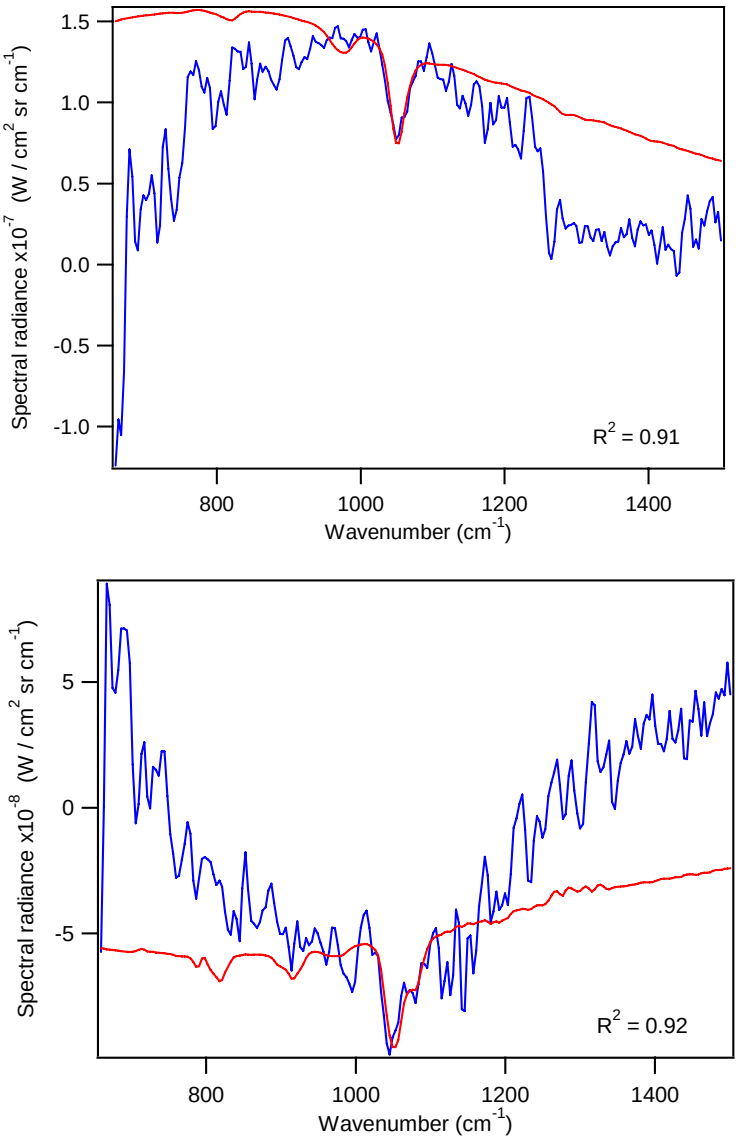

Figure 29: Comparison of the best-fit spectrum of a DMMP-TEP simulation (red curve) with the measured differential radiance spectrum (blue curve) at 88 s (top) and 131 s (bottom) after the release began.

Figure 30 shows a plot of the goodness of fit (r^2) and the column density (CL) of DMMP and TEP vapour as a function of time determined from the GASEM fitting procedure. The fit was obtained with a filling factor estimated at 50% and the chemical gas temperature was adjusted 1.5K lower than the air temperature to obtain the best fit. The fluctuation in the goodness of fit can be attributed to the FOR scanning procedure.

The SNR for these measurements was sufficient to detect and identify the DMMP-TEP vapour mixture at a distance of 1515 m.

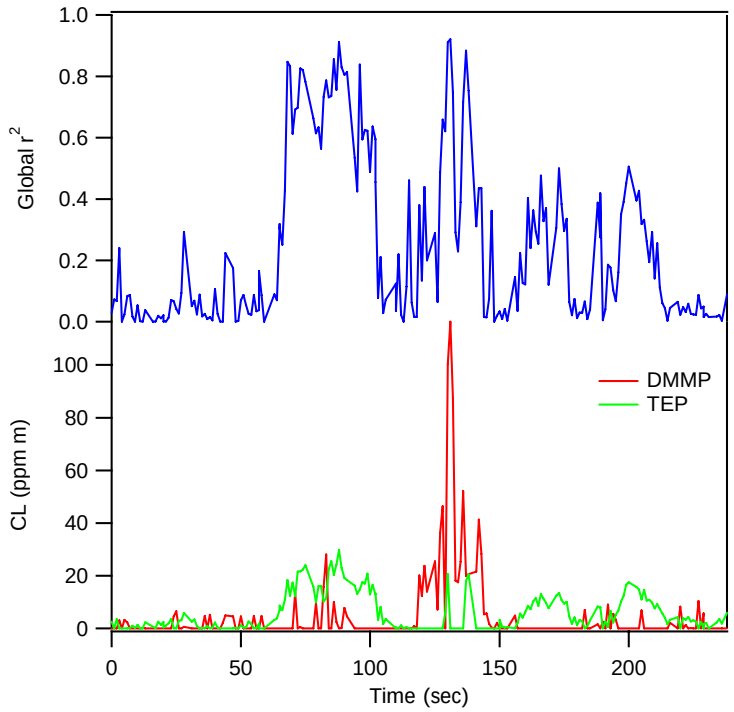

Figure 30: Plot of the goodness of fit (r^2) and the column density (CL) of a DMMP-TEP mixture determined from the GASEM fitting procedure

4.3 Toxic industrial chemicals

Two types of release methods were used to disseminate the TICs. One approach involved the controlled release of the gas directly from a tank through a valve, and the second method consisted of detonating explosive ribbons wrapped around a gas cylinder to achieve an instantaneous release.

4.3.1 Phosgene: controlled release

Figure 31 shows the results obtained for a release of phosgene at a rate of 1.2 kg/min for 3 min at a distance of 870 m from the sensor. The overlay plot and the spectrogram of the differential radiance show all the spectra measured by CATSI during the release time, which was 12:13 LT on June 13, 2005. The background for this measurement consisted mostly of grass, and the temperature contrast was evaluated at about 1.1 K. The spectrogram in the 800–900 cm^{-1} region clearly shows the evolution of the phosgene band over time with a sufficient SNR to permit detection of the gas in the interval between 60 and 240 s.

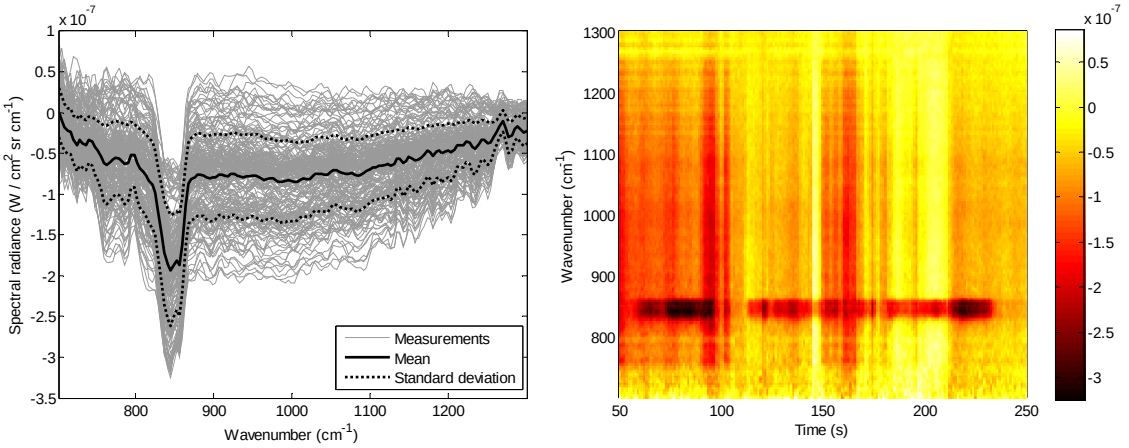

Figure 31: Phosgene release experiment (1.2 kg/min). Evolution of the measured differential radiance in different projections; overlay plot of the radiance acquired by CATSI (left), and spectrogram showing the radiance as a function of time (right).

Figure 32 shows the best fit between the phosgene spectrum computed with the GASEM model (red curve) and the measured differential radiance at 218 s after the release began. The comparison of the fitted signature and the measured spectrum gives a fit quality of 0.98. The bottom part of Figure 32 shows a plot of the goodness of fit (r^2) and the column density (CL) of phosgene as a function of time determined from the GASEM fitting procedure. The fit was obtained with a filling factor estimated at 90% and the chemical gas temperature was adjusted 1.3K lower than the air temperature to achieve a better fit. The fluctuation in the column density and the goodness of the fit can be attributed to the FOR scanning procedure.

The SNR for these measurements was sufficient to permit a clear detection and identification of phosgene with a fit quality of about 0.90 when the gas cloud was present within the FOV. This clearly illustrates that CATSI can detect and identify phosgene vapours at a distance of 870 m. At this distance the FOV is approximately 7 m, and it can be determined from Figure 33 that the FOV is mostly filled by the release plume if the sensor is pointed near the release point.

Figure 33 presents a plume dispersion of phosgene at 1.25 kg/min and a wind speed of 3 m/s. In order to verify the CL value calculated with the GASEM algorithm, an average CL value was calculated over the CATSI FOV from the plume simulation. For this simulation, a column density of 380 ppm m was calculated and it can be compared with the measured CL presented in Figure 32. The comparison shows that the measured CL is consistent with the result obtained from the plume model simulation.

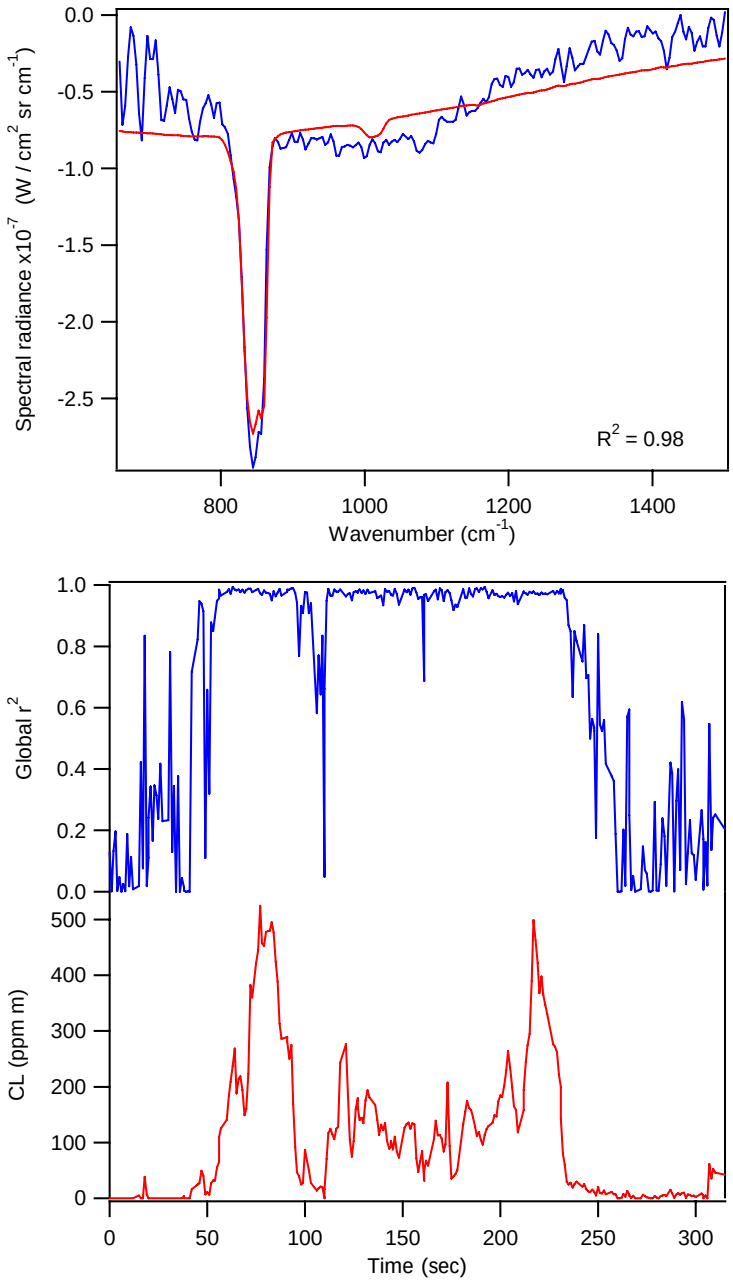

Figure 32: Comparison of the best-fit phosgene simulation (red curve) with the measured differential radiance spectrum (blue curve) at 218 s after the release began (top). Plot of the goodness of fit (r^2) and the column density (CL) of phosgene determined from the GASEM fitting procedure (bottom).

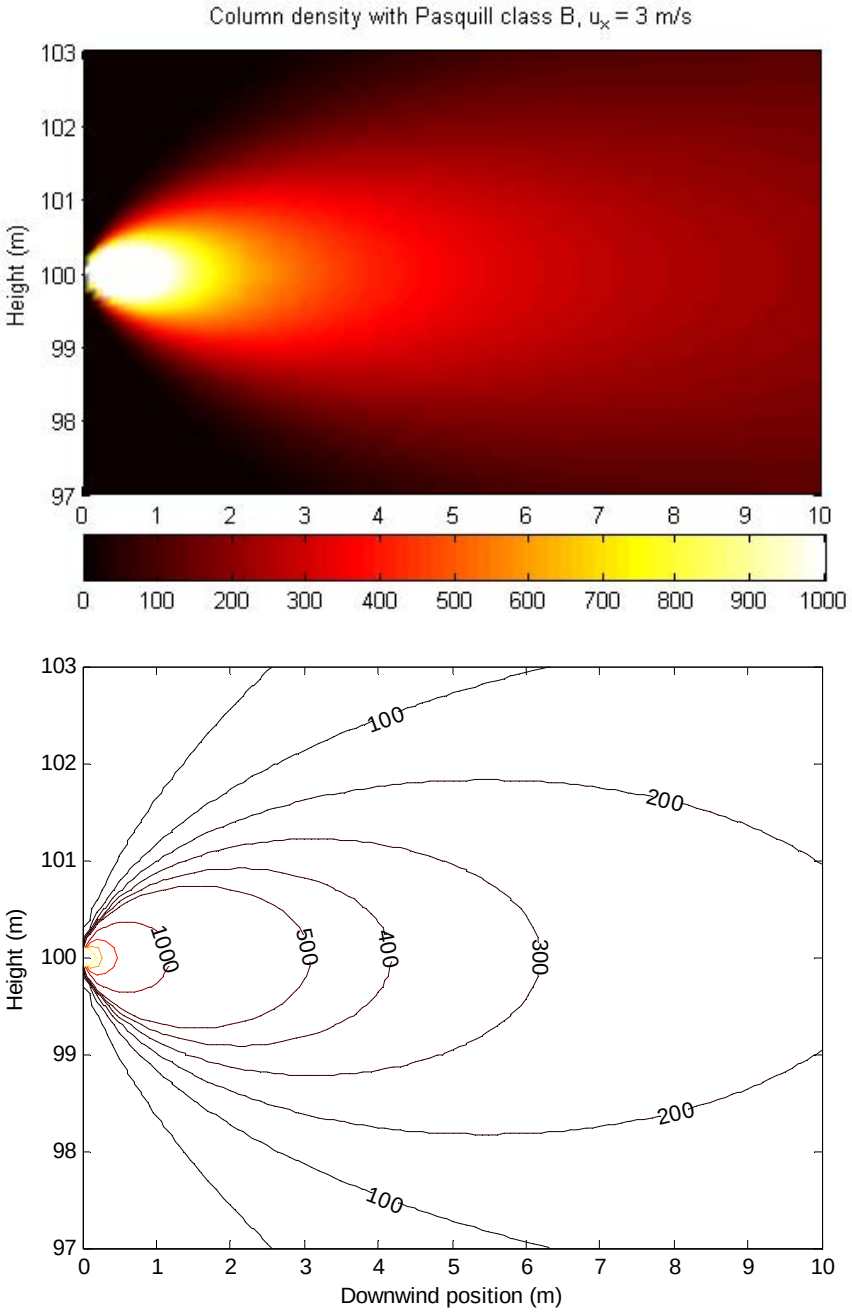

Figure 33: Gaussian plume simulation of a phosgene release at 1.2 kg/min. The lower figure presents the column density (CL in ppm m) as a function of distance.

4.3.2 Phosgene: explosive release

Figure 34 shows the results obtained for an instantaneous release of 6 kg of phosgene at 870 m from the sensor. The overlay plot and the spectrogram of the differential radiance show all the spectra collected by CATSI during the release time, which was 14:05 LT on June 17, 2006. The background for this measurement consisted mostly of grass, and the temperature contrast was evaluated at about 1.1 K.

During the measurement period, both positive and negative phosgene bands could be observed, as shown in the overlay plot (Figure 34). The positive signal was observed just after the explosion and is attributed to a chemical vapour with a temperature higher than the air. After about 100 s the signal became negative and this is associated with phosgene gas at a temperature lower than the background. The period between 90 and 100 s when no signal was observed could be attributed to the time when the chemical vapour was at the same temperature as the background, or when the gas was not in the sensor FOV. The spectrogram in the 800–900 cm^{-1} region clearly shows the evolution of the phosgene band over time with a sufficient SNR to permit detection in the interval between 80 and 185 s.

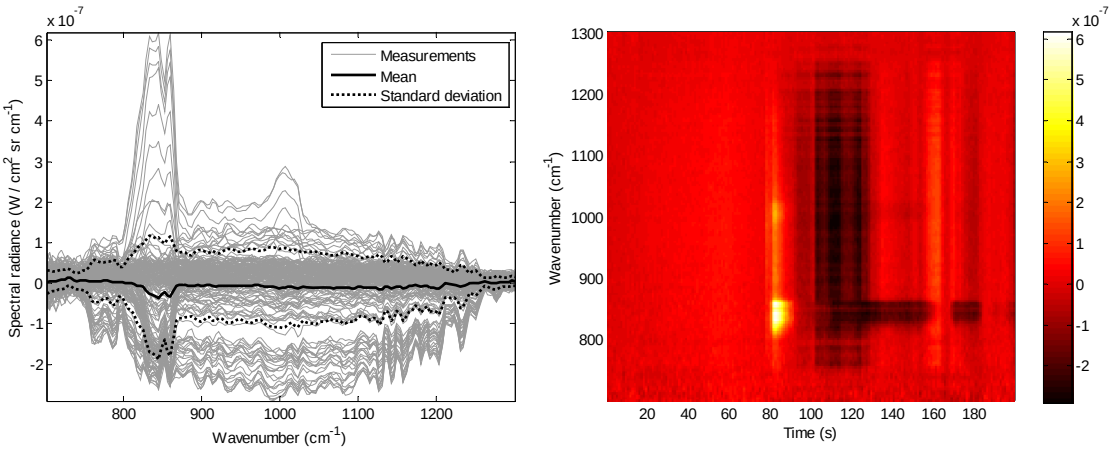

Figure 34: Explosive phosgene experiment (release of 6 kg). Evolution of the measured differential radiance in different projections; overlay plot of the radiance acquired by CATSI (left), and spectrogram showing the radiance as a function of time (right).

Figure 35 shows the best fit between the phosgene spectrum computed with the GASEM model (red curve) and the measured differential radiance at 82 s (top) and 153 s (bottom) after the spectral collection began. The comparison of the fitted signatures and measured spectra results in a fit quality of 0.95 and 0.90, respectively. The upper graph in Figure 35 shows the presence of a continuum offset, which can be explained by the gas cloud at a higher temperature acting as a blackbody radiator shortly after the explosion. Figure 36 shows an IR image of the scene at 1 s after detonation, and the explosion can be clearly distinguished by its higher temperature (red circle).

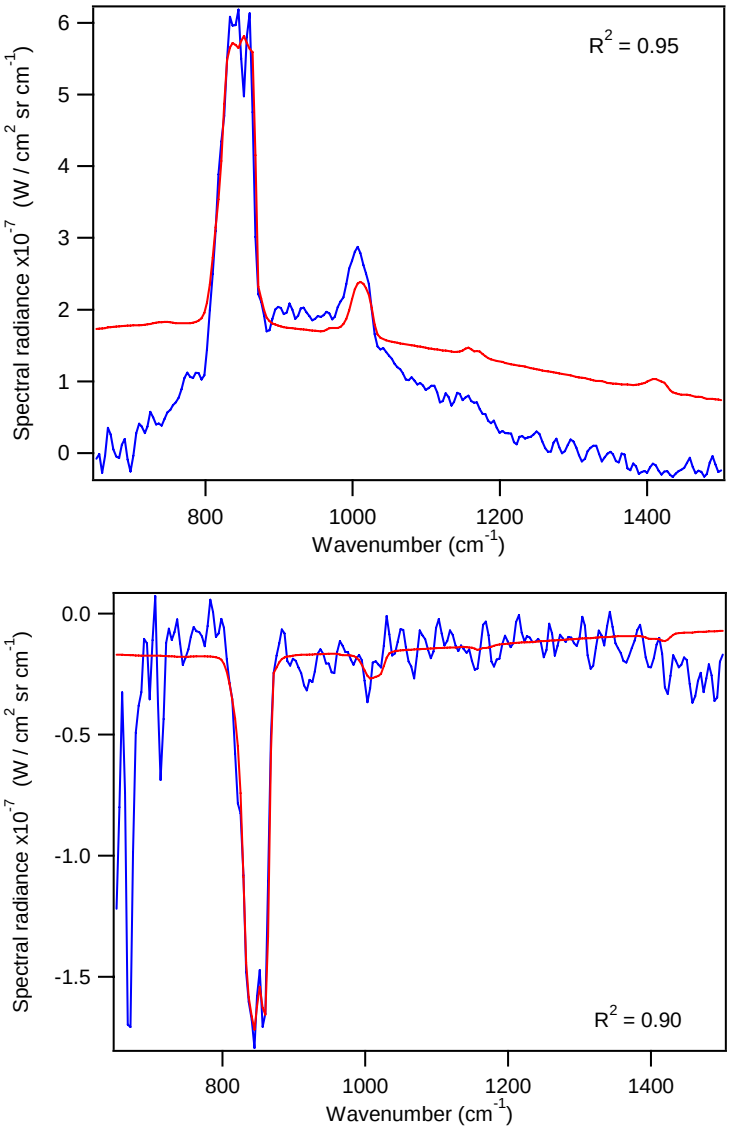

Figure 35: Comparison of the best-fit spectrum of a phosgene simulation (red curve) with the measured differential radiance spectrum (blue curve) at 82 s (top) and 153 s (bottom) after the release began.

Figure 36: Infrared (8-12μm) image of the phosgene instantaneous release.

Figure 37 shows the results obtained for an instantaneous release of 3 kg of phosgene at 1530 m from the sensor. The overlay plot and the spectrogram of the differential radiance show all the spectra collected by CATSI during the release, which occurred at 15:40 LT on June 28, 2005. The background for this measurement consisted mostly of grass, and the temperature contrast was evaluated at about -3.4 K. The overlay plot shows some spectra containing features associated with a sky background. This occurred when the CATSI sensor was pointed above the trees beyond the valley (Figure 36).

In contrast to Figure 34, this measurement shows only a positive signal. This indicates that the phosgene cloud temperature was always higher than the background over the time of the experiment. In this case the FOV of the sensor included a significant sky background contribution, which represents a cold source. The spectrogram in the 800–900 cm^{-1} region clearly shows the evolution of the phosgene band over time with a sufficient SNR to permit detection in the interval between 65 and 125 s.

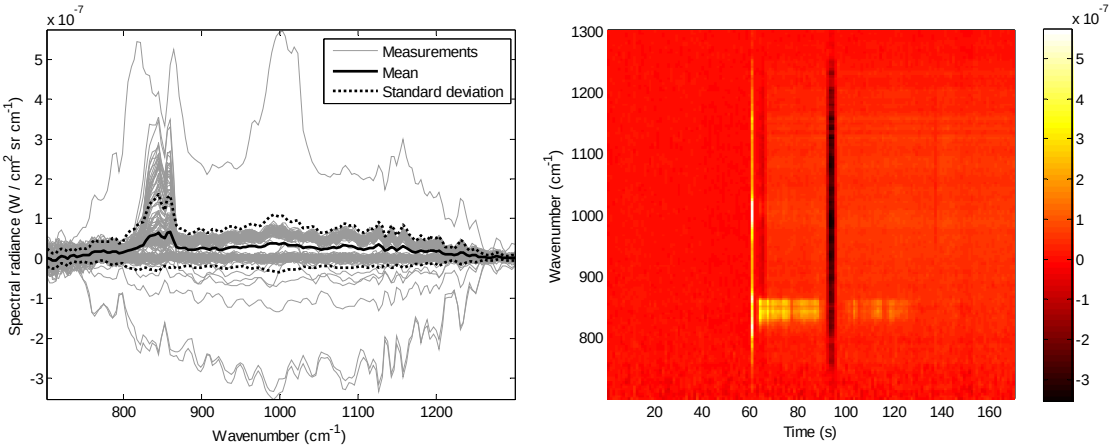

Figure 37: Explosive phosgene experiment (release of 3 kg). Evolution of the measured differential radiance in different projections; overlay plot of the radiance acquired by CATSI (left), and spectrogram showing the radiance as a function of time (right).

Figure 38 shows the best fit between the phosgene spectrum computed with the GASEM model (red curve) and the measured differential radiance at 67 s after the spectral collection began. The comparison of the fitted signature with the collected spectrum gives a fit quality of 0.94.

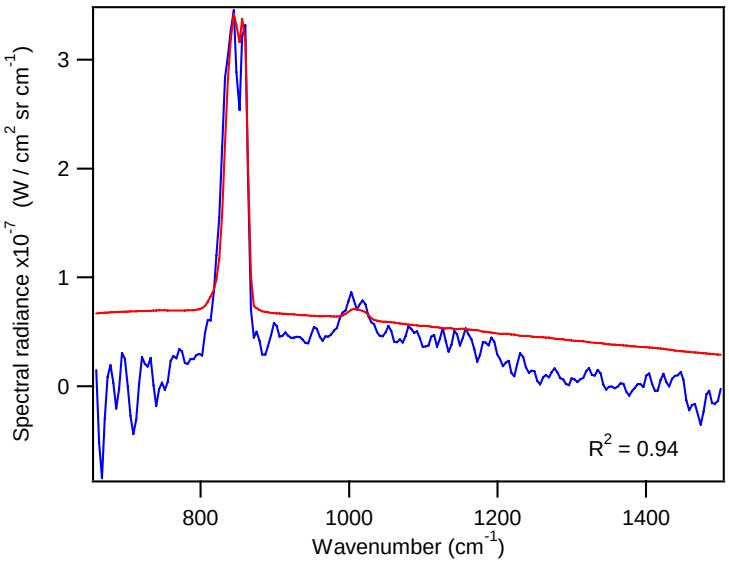

Figure 38: Comparison of the best-fit spectrum of a phosgene simulation (red curve) with the measured differential radiance spectrum (blue curve) at 67 s after the release began.

4.4 Chemical warfare agent

Figure 39 shows spectral measurements for a small release of GB at a distance of 485 m from the sensor at 19:05 LT on June 30, 2005. A total of 150 g of GB was released inside the cloche and the resulting vapour cloud was extracted with a fan positioned at the front end of the cloche. Figure 39 shows the best fit between the GB spectrum computed with the GASEM model (red curve) and the measured differential radiance at 232 s (top) and 234 s (bottom) after the release began. The comparison of the fitted signature and the collected spectrum gives a fit quality of 0.21 (top) and 0.23 (bottom). The SNR observed during this measurement was approximately 2, and the result was an adequate signal for the detection algorithms to detect and identify the GB. The overlay plot and the spectrogram for this experiment are not presented, since the SNR is not sufficient to distinguish the GB features from the background clutter.

Figure 40 shows a plot of the goodness of fit (r^2) and the column density (CL) of GB vapour as a function of time determined from the GASEM fitting procedure. This figure demonstrates that CATSI could detect and identify GB vapour at low concentration from a distance of 485 m. The global fit quality is low compared with the measurements for the other simulants; however, it was sufficient to determine whether or not GB was present in the measurement (Figure 40). The fitting procedure indicated that, for the GB release, the temperature of the vapour in the CATSI sensor FOV was roughly 2.5 K higher than the air temperature. This temperature difference made it difficult for GASEM to model the collected signal, but a suitable choice of environmental parameters during post-processing yielded a significant increase in fit quality. This temperature difference could be explained by the method of dissemination in which the CWA inside the cloche was heated by the sun shining on the surrounding enclosure so that it was warmer than the air on release.

Figure 41 presents a plume dispersion of GB at 0.150 kg/min and at a wind speed of 4 m/s. At a distance of 485 m the FOV was approximately 4 m, and it can be determined from Figure 41 that the FOV was mostly filled by the release plume when the sensor was pointed near the release point. In order to verify the CL value calculated with the GASEM algorithm, an average CL value was calculated over the CATSI FOV from the plume simulation. For this simulation, a column density of 25 ppm m was calculated and it can be compared with the measured CL presented in Figure 40. This is consistent with the column density obtained with the GASEM fitting procedure.

Figure 42 shows simulations performed with the Line-by-Line Radiative Transfer Model (LBLRTM) [12] incorporating the same atmospheric and concentration parameters as the experiment, and at three different values of ΔT. The simulations show that the differential radiance observed in Figure 39 is the same order of magnitude as the signal modelled for a cloud with a column density of 13 ppm m and a ΔT of 1 to 1.5 K. Hence, this suggests that the measured GB result is reasonable given the atmospheric parameters of the field experiment.

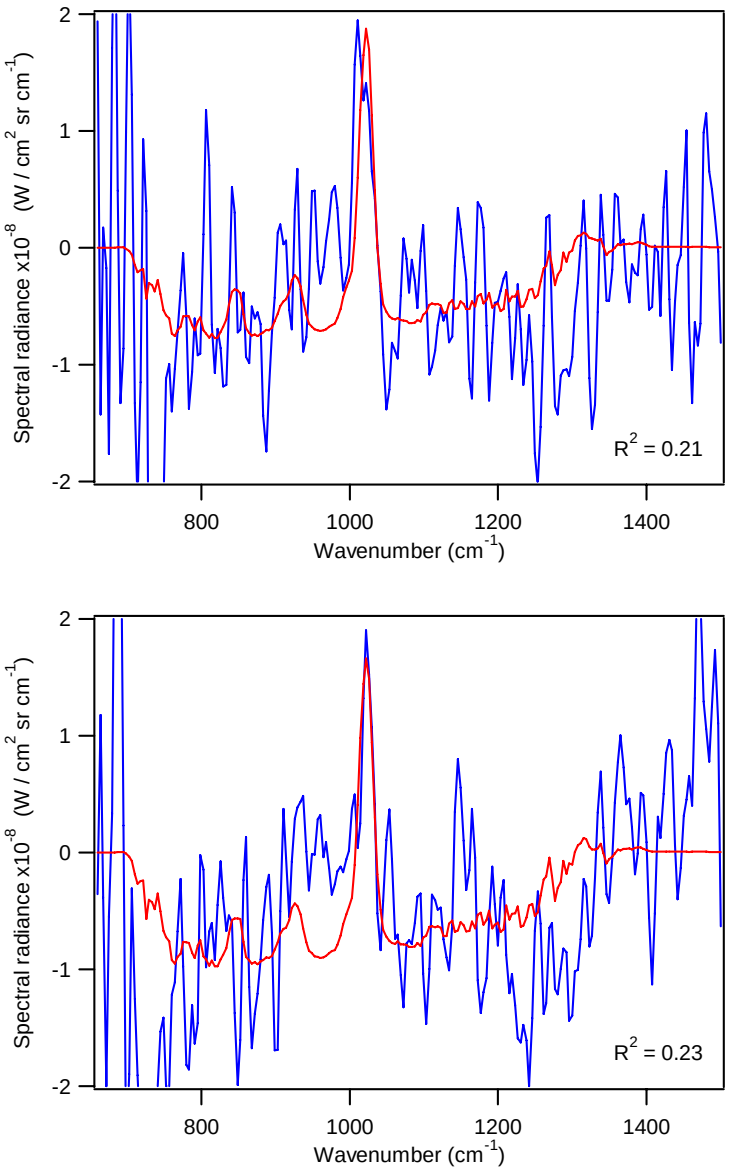

Figure 39: Result of the best-fit GB simulation (red curve) with the measured differential radiance spectrum (blue curve) at 232 s (top) and 234 s (bottom) after the release began.

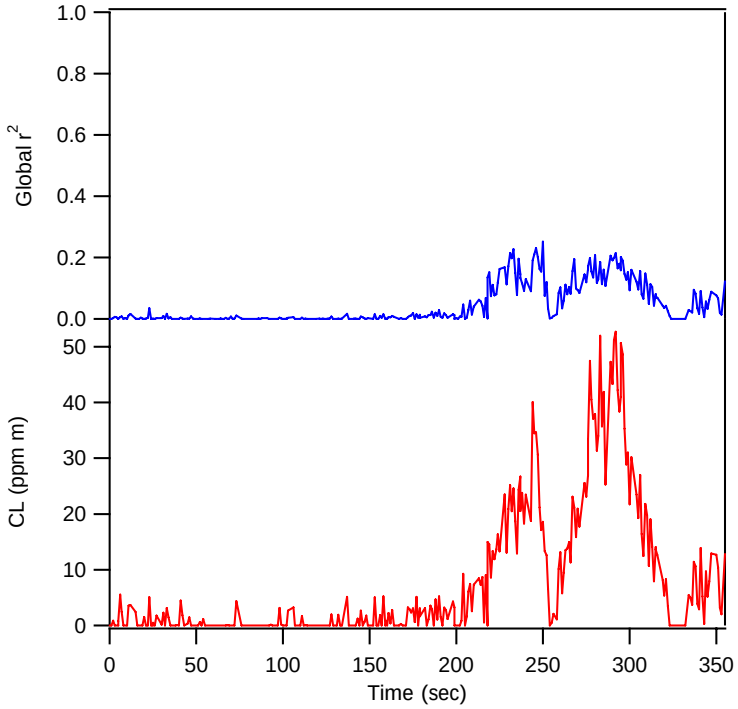

Figure 40: Plot of the goodness of fit (r^2) and the column density (CL) of GB determined from the GASEM fitting procedure.

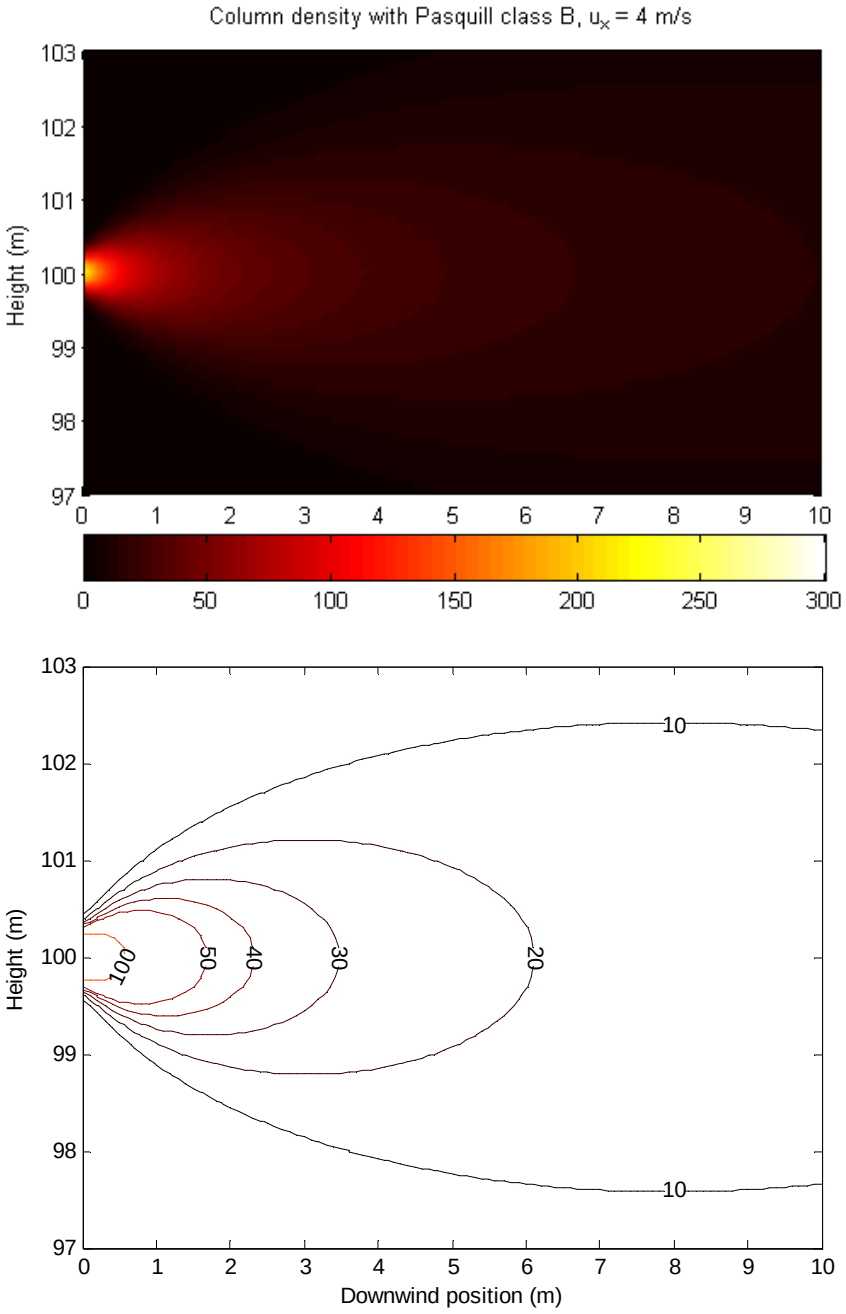

Figure 41: Gaussian plume simulation of a GB release at 0.15 kg/min. The lower figure presents the column density (CL in ppm m) as a function of distance.

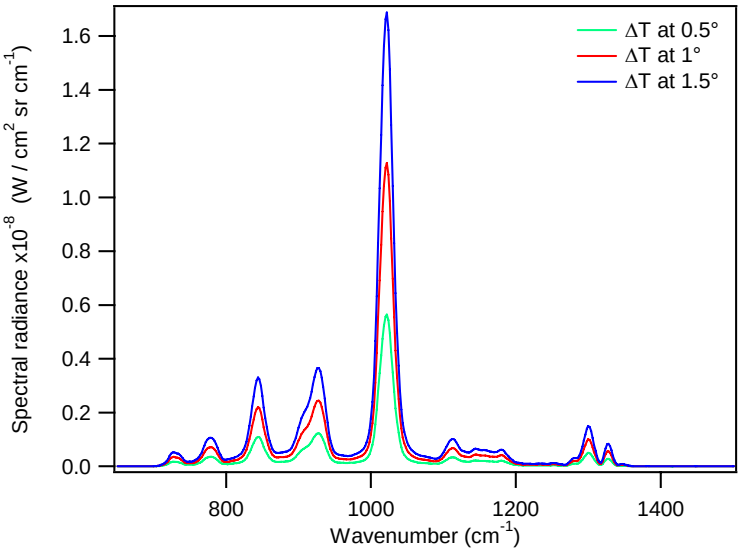

Figure 42: Simulation of GB spectrum performed at three different ΔT with a column density of 75 mg/m^2 (13 ppm m).

Figure 43 shows the concentration of a plume of GB simulated for a release rate of 0.15 kg/min and a wind speed of 4 m/s. This simulation was performed to validate the Gaussian plume model by comparing with the measured GB concentrations from point sensors distributed over the open-air range during the release. Table 2 shows the concentrations measured by three point sensors (PPBRae type sensors) used for ground-truth measurements during the GB release experiments on June 30 at 19:05 LT. The Gaussian plume simulation presented in Figure 43 is identical to the simulation shown in Figure 41; however, the concentration values (in ppmv) are shown instead of the CL values (in ppm m). The measurements from the point sensors (in mg/m^3) were converted to ppmv to compare with the Gaussian plume results presented on Figure 43. The comparison shows that the result obtained with the first point sensor was 2 to 3 times lower than the simulated values, and the results obtained with point sensors 2 and 3 were consistent with the simulated values. This comparison shows that the plume dispersion simulated with the Gaussian model provides GB concentrations consistent with the measured values, and it is, therefore, an acceptable method for comparing with the CL values derived from the CATSI measurements.

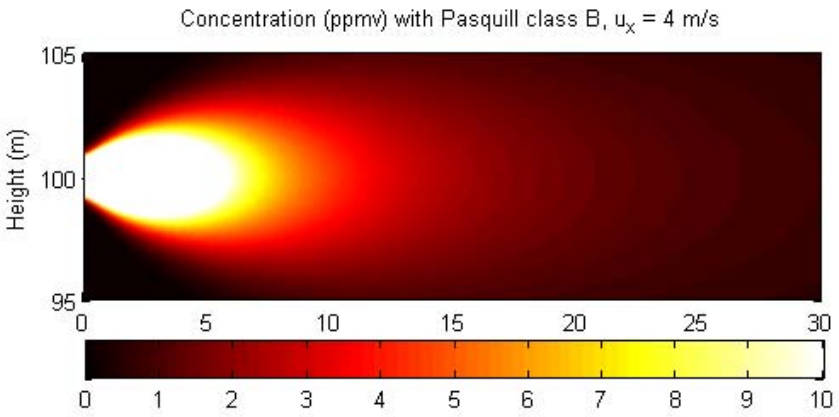

Figure 43: Gaussian plume simulation of GB concentration (ppmv) from a release at a rate of 0.15 kg/min

Table 2: *Position of the chemical point sensors used in the ground-truth grid position.*

Sensor number	Distance (m)	Measured concentration (mg/m^3)	(ppmv)	Simulated concentration[1] (ppmv)
1	11	8.8	1.4	3.0 to 4.5
2	19.5	6.1	1.0	1.5 to 2.0
3	27	4.6	0.75	1.0

[1] Concentration estimated from the Gaussian plume simulation.

5. Conclusion

This report summarizes the results measured for several chemical vapours at standoff distances of 500 m to 1.5 km using the passive LWIR sensor CATSI. These measurements were performed at DSTL, Porton Down, UK in June 2005 and they included simulants and precursors of CWAs, TICs and one real CWA.

The measurements performed in this open-air environment provided clear evidence that passive standoff LWIR sensors can detect and identify real CWA vapours released at low concentration (approx. 150 g in 120 s) and low thermal contrast. These results provide evidence that the environment does not significantly alter the signature of toxic chemical vapours from their pure state.

The greatest difficulty encountered in this field trial was the low temperature contrast (ΔT) resulting from the grassy terrain. Only 25% of the observed temperature contrasts were higher than 1.0 K; normally, one would expect to encounter contrasts of several degrees from other terrain types.

The explosive releases of toxic chemical vapours (phosgene) provided good detection results and demonstrated the capability of the CATSI sensor to detect and identify a toxic chemical cloud dispersed instantaneously. These results are of military importance since they approximate the real conditions that may be encountered on the battlefield or from a terrorist threat.

In addition, this work provided some evidence that yellow smoke used as an obscurant to mask the chemical vapour will not affect the identification process but may reduce detectability. Hence, the use of battlefield obscurants lacking a significant signature (grey body) may not dramatically affect the performance of a LWIR passive sensor such as CATSI.

This field trial provided an exceptional opportunity to increase the level of knowledge and confidence concerning the detection and identification limits of chemical vapours.

References

[1] Lavoie, H., E. Puckrin, J.-M. Thériault, and F. Bouffard (2005) *Passive standoff detection of SF6 at a distance of 5.7 km by differential FTIR radiometry.* Appl. Spectros., **59**(10): p. 1189-1193(5).

[2] Thériault, J.-M. (2001) *Passive Standoff Detection of Chemical Vapors by Differential FTIR Radiometry*. DREV Technical Report, **TR-2000-156**.

[3] Thériault, J.-M., C. Bradette, A. Villemaire, M. Chamberland, and J. Giroux (1997) *Differential detection with a double-beam interferometer, in Electro-optical Technology for Remote Chemical Detection and Identification II.* SPIE Proc., **3082**: p. 65-75.

[4] Thériault, J.-M. and E. Puckrin (2005) *Remote sensing of chemical vapours by differential FTIR radiometry*. Int. J. Remote Sens., **26**: p. 981-995.

[5] Thériault, J.-M., E. Puckrin, F. Bouffard, and B. Déry (2004.) *Passive Remote Monitoring of Chemical Vapors by Differential FTIR Radiometry: Results at a Range of 1.5 km.* Appl. Opt., **43**: p. 1425-1434.

[6] Thériault, J.-M., E. Puckrin, J. Hancock, P. Lecavalier, C.J. Lepage, and J.O. Jensen (2004) *Passive standoff detection of chemical warfare agents on surfaces.* Appl. Opt., **43**: p. 5870-5885.

[7] Theriault, J.-M., E. Puckrin, and J.O. Jensen (2003) *Passive standoff detection of BG aerosol by FTIR radiometry.* Appl. Opt., **41**: p. 6696-6705.

[8] Thériault, J.-M. (1999) *Modeling the Responsivity and Self-emission of a Double-beam Fourier-transform infrared interferometer.* Appl. Opt., **38**: p. 505-515.

[9] Jones, A.W. (2005) *Field trials protocol: Passive stand-off detection of CW agent, Toxic industrial chemicals and simulant vapours.* DSTL Report, **DSTL/WP15178**.

[10] Pasquill, F. (1961) *The estimation of the dispersion of windborne material.* Meteorol. Mag., **90**: p. 33-49.

[11] Seinfeld, J.H. and S.N. Pandis, *Air Pollution, Physical and Chemical Fundamentals*. 1998, New York: McGraw-Hill. Ch. 18.

[12] Clough, S.A. and M.J. Iacono, *Line-by-line calculations of atmospheric fluxes and cooling rates 2: Application to carbon dioxide, ozone, methane, nitrous oxide and the halocarbons.* J. Geophys. Res., 1995. **100**: p. 16519-16535.

This page intentionally left blank.

List of symbols/abbreviations/acronyms/initialisms

CATSI	Compact ATmospheric Sounding Interferometer
CL	Column density
CF	Canadian Forces
CG	Phosgene
CWA	Chemical Warfare Agent
ΔT	Thermal contrast
DMMP	DiMethylMethyl-Phosphonate
FOR	Field Of Regard
FOV	Field Of View
GASEM	GASeous Emission Monitoring
GB	Sarin
K	Kelvin (degree)
LT	Local Time
LWIR	Long Wave InfraRed
DND	Department of National Defence
DSTL	Defence Science and Technology Laboratory
NH_3	Ammonia
ppm	Part(s) Per Million
R&D	Research & Development
SF_6	Sulphur hexafluoride
SNR	Signal-to-Noise Ratio
TEP	TriEthyl Phosphate
TIC	Toxic Industrial Chemical

This page intentionally left blank.

Distribution list

Document No.: DRDC Valcartier TR 2006-634

LIST PART 1: Internal Distribution by Centre:

1 - Director General
3 - Document Library
1 - H. Lavoie (author)
1 - E. Puckrin (author)
1 - J.-M. Thériault (author)
1 - D. Dubé (author)
1 - Hd/SOp
1 - Hd/GEO
1 - J.-P. Ardouin
1 - F. Bouffard
1 - G. Roy
1 - J.-R. Simard
1 - T. Smithson
1 - C.S. Turcotte

TOTAL LIST PART 1 16

LIST PART 2: External Distribution by DRDKIM

1 - DRDKIM (unbound copy)
1 - DRDC
1 - DRDC Ottawa
1 - DRDC Atlantic
1 - DRDC Suffield
1 - DRDC Toronto
1 - Director Science and Technology (Command and Control Information Systems)
1 - Director Science and Technology (Land)
1 - Director Science and Technology (Policy)
1 - Director Science and Technology (Maritime)
1 - Director Science and Technology (Air)
1 - Director Science and Technology (Human Performance)
1 - J2 DSI (Directorate Strategic Information)
1 - Lcol Rick Barker
DNBCD 2
NucBioChem Def Capability Development National
Defence Headquarters
101 Colonel By Drive
Ottawa, ON
K1A 0K2
1 - Dr. James O. Jensen
U.S. Army SBCCOM
ATTN: SCBRD-RTE
Building E3549, Room C236
Aberdeen Proving Ground, MD 21010-5423
U.S.A.
1 - Major Johanne Côté
DNBCD 2-4
Detection & Identification - Chem & Rad
National Defence Headquarters
101 Colonel By Drive
Ottawa, ON
K1A 0K2

TOTAL LIST PART 2 16

TOTAL COPIES REQUIRED 32

DOCUMENT CONTROL DATA

(Security classification of title, body of abstract and indexing annotation must be entered when the overall document is classified)

1. ORIGINATOR (The name and address of the organization preparing the document. Organizations for whom the document was prepared, e.g. Centre sponsoring a contractor's report, or tasking agency, are entered in section 8.)

DRDC Valcartier

2. SECURITY CLASSIFICATION (Overall security classification of the document including special warning terms if applicable.)

3. TITLE (The complete document title as indicated on the title page. Its classification should be indicated by the appropriate abbreviation (S, C, R or U) in parentheses after the title.)

Measurement of toxic industrial chemicals, chemical warfare agent and their simulants: A LWIR passive standoff detection study

4. AUTHORS (last name, followed by initials – ranks, titles, etc. not to be used)

Lavoie, H., E. Puckrin, J.-M. Thériault and D. Dubé

5. DATE OF PUBLICATION (Month and year of publication of document.)

April 2007

6a. NO. OF PAGES (Total containing information, including Annexes, Appendices, etc.)

82

6b. NO. OF REFS (Total cited in document.)

9

7. DESCRIPTIVE NOTES (The category of the document, e.g. technical report, technical note or memorandum. If appropriate, enter the type of report, e.g. interim, progress, summary, annual or final. Give the inclusive dates when a specific reporting period is covered.)

Technical Report

8. SPONSORING ACTIVITY (The name of the department project office or laboratory sponsoring the research and development – include address.)

DNBCD-DSSPM

9a. PROJECT OR GRANT NO. (If appropriate, the applicable research and development project or grant number under which the document was written. Please specify whether project or grant.)

16qk

9b. CONTRACT NO. (If appropriate, the applicable number under which the document was written.)

10a. ORIGINATOR'S DOCUMENT NUMBER (The official document number by which the document is identified by the originating activity. This number must be unique to this document.)

DRDC Valcartier TR 2006-634

10b. OTHER DOCUMENT NO(s). (Any other numbers which may be assigned this document either by the originator or by the sponsor.)

11. DOCUMENT AVAILABILITY (Any limitations on further dissemination of the document, other than those imposed by security classification.)

(X) Unlimited distribution
( ) Defence departments and defence contractors; further distribution only as approved
( ) Defence departments and Canadian defence contractors; further distribution only as approved
( ) Government departments and agencies; further distribution only as approved
( ) Defence departments; further distribution only as approved
( ) Other (please specify):

12. DOCUMENT ANNOUNCEMENT (Any limitation to the bibliographic announcement of this document. This will normally correspond to the Document Availability (11). However, where further distribution (beyond the audience specified in (11) is possible, a wider announcement audience may be selected.))

[Document Announcement]

13. ABSTRACT (A brief and factual summary of the document. It may also appear elsewhere in the body of the document itself. It is highly desirable that the abstract of classified documents be unclassified. Each paragraph of the abstract shall begin with an indication of the security classification of the information in the paragraph (unless the document itself is unclassified) represented as (S), (C), (R), or (U). It is not necessary to include here abstracts in both official languages unless the text is bilingual.)

This report presents a summary of the measurements performed using the Compact Atmospheric Sounding Interferometer (CATSI) for the standoff detection of toxic chemical vapours at DSTL, Porton Down, UK in June 2005. This work is based on the passive standoff detection of chemical warfare agent (CWA) simulants, such as SF_6, NH_3, and TEP, precursors, such as DMMP, and toxic chemical vapours, such as phosgene and GB. The measurements were performed for a variety of concentrations and at low thermal contrast in an open-air environment. Some chemicals were released in the presence of yellow smoke to act as an obscurant. The measurements collected during the trial have been used to evaluate the performance and capacity of the CATSI sensor for detecting, identifying and quantifying a chemical vapour cloud at a distance between 500 m to 1.5 km. The results show that CATSI was able to detect and identify all of the chemical vapours, including the CWA, released during the trial. The measurements made in the presence of yellow smoke provide some preliminary evidence that some obscurants do not significantly affect the detection capability of a passive standoff sensor. The measurements of GB in the field also demonstrate that the real atmosphere has an insignificant effect on the signature of the pure agent. The work performed in this field trial is also useful for validating the approach and methodology used in the new engineering development model of the CATSI system (CATSI-EDM), which will be made available to the CF in 2007.

14. KEYWORDS, DESCRIPTORS or IDENTIFIERS (Technically meaningful terms or short phrases that characterize a document and could be helpful in cataloguing the document. They should be selected so that no security classification is required. Identifiers, such as equipment model designation, trade name, military project code name, geographic location may also be included. If possible keywords should be selected from a published thesaurus, e.g. Thesaurus of Engineering and Scientific Terms (TEST) and that thesaurus identified. If it is not possible to select indexing terms which are Unclassified, the classification of each should be indicated as with the title.)

CATSI, Chemical Agent Detection, LWIR sensor, Passive standoff, Differential FTIR radiometry

Defence R&D Canada

Canada's Leader in Defence
and National Security
Science and Technology

R & D pour la défense Canada

Chef de file au Canada en matière
de science et de technologie pour
la défense et la sécurité nationale

WWW.drdc-rddc.gc.ca